The Seasonal Evolution of Subglacial Drainage Pathways Beneath a Soft-bedded Glacier

Jane Hart (jhart@soton.ac.uk)
Geography and Environmental Science, University of Southampton, Southampton, SO17 1BJ, 5 UK
David Young
University of Southampton
Nathaniel Baurley
University of Southampton
Benjamin Robson
University of Bergen
Kirk Martinez
University of Southampton

Research Article

Keywords: Subglacial hydrology, unconsolidated sedimentary, West Antarctica, glacier speed-up events

Posted Date: January 23rd, 2021

DOI: https://doi.org/10.21203/rs.3.rs-150732/v1

The seasonal evolution of subglacial drainage pathways beneath a soft-bedded glacier

Jane K. Hart*[1], David S. Young [2], Nathaniel Baurley[1], Benjamin Robson[3] and Kirk Martinez [2]

[1]*Geography and Environmental Science, University of Southampton, Southampton, SO17 1BJ, UK*

[2]*Electronics and Computer Science, University of Southampton, Southampton, SO17 1BJ, UK*

[3]*Department of Earth Science, University of Bergen, 5020 Bergen, Norway*

Corresponding author: Jane K. Hart (jhart@soton.ac.uk)

Abstract

Subglacial hydrology is a key element in glacier response to climate change, but investigations of this environment are logistically difficult. Most models are based on summer data from glaciers resting on rigid bedrocks. However a significant number of glaciers rest on soft (unconsolidated sedimentary) beds, including the potentially unstable ice streams of West Antarctica. Here we present a rare multi-year instrumented record of the development of seasonal subglacial behavior in a temperate glacier resting on a deformable sediment layer as an analogue for West Antarctica. We observe a distinct annual pattern in the subglacial hydrology based on self-organizing anastomosing braided channels. Water is stored within the subglacial system itself (till, braided system and 'ponds'), allowing the rapid access of water to enable glacier speed-up events to occur throughout the year, particularly in winter.

Introduction

Recent accelerated climate change has led to rapid glacier retreat, which is thought to be a significant component of future sea level[1]. Two key unknown elements used in ice-sheet models for sea level prediction include an understanding of subglacial hydrology and sediment deformation[2, 3, 4]; and it has been shown that the use of different sliding laws results in very different outcomes[5, 6].

Most models of subglacial hydrology assume a hard bedrock system dominated by conduits, linked cavities and films[7]. In these models, winter is characterised by an inefficient distributed system, with low surface velocity and generally high water pressures[8, 9, 10]. In the spring, warming temperatures cause the meltwater input to be higher than drainage capacity, leading to water pressure rising higher than overburden pressure and resultant basal sliding (the 'spring event') associated with the transition from one system to the other [11, 12, 13]. Summer is dominated by high velocities and low water pressure and an efficient channelized system.

Recent research from Greenland has shown that in early summer whenever there are large surface melt events, water is able to reach the glacier base, leading to increased velocities via basal sliding[14, 15]. However, in late summer, glacier velocity is not directly related to meltwater input because once the system is channelised, additional meltwater can be accommodated (self-regulation) by the subglacial hydrological system[16, 17]. This system drains both 'connected' core areas comprising efficient channels, surrounded by 'weakly connected' areas comprising distributed drainage[18, 19, 20, 21].

However, this model may not be universal. Glaciers resting on soft beds have a different hydrology dominated by wide anastomosing broad flat channels, canals, macroporous films

45 (at the ice/sediment interface) and porous flow through the till[22, 23, 24], resulting in a complex
46 relationship between till water pressure, basal sliding and deformation[25, 26, 27, 28]. Much of this
47 system has been characterized as an inefficient or distributed system[2, 29], although numerous
48 researchers[21, 30] have argued that canals can be both efficient[31] and inefficient[23].

49 This is important because unconsolidated sediments are found beneath many of the fast
50 flowing ice streams of Antarctica and parts of Greenland, as well as in areas covered by the
51 Quaternary ice sheets during previous glaciations[4, 32, 33, 34, 35].

52 The majority of studies (both field and theoretical) have concentrated on rigid-bedded
53 glaciers, and summer data. We present a rare instrumented multi-year, seasonal data set of a
54 soft-bedded glacier, from which we reconstruct subglacial drainage patterns throughout the
55 year. Each year, summer melt represents only 50% of discharge. This excess water goes into
56 storage within the subglacial system, where it is held within a wide and shallow
57 anastomosing system of active and less active channels, as well as the macroporous and till
58 layer. In late autumn the number of channels decreases and the reservoirs become isolated.
59 During winter, discharge represents almost five times the melt, and on warm days when
60 melting occurs, melt water is rapidly transported to the glacier bed which leads to basal
61 sliding, bed separation and water pressure decline. This uplift of the glacier allows these
62 subglacial reservoirs to be accessed, leading to a continued period of high drainage long after
63 the melt-driven event has ceased, as well as a rearrangement of the drainage system until the
64 next event occurs.

65 In Spring, melt increases until it overwhelms the capacity of the winter drainage system,
66 resulting in 'Spring Events', which are similar to the winter events, but which lead to the
67 development of a new drainage system which is able to cope with the increased level of melt
68 entering the system'. As melt increases through the summer, so does the level of

anastomosing, with resulting high water pressures, increasing accommodation of melt events, and the development of storage within the subglacial system itself. We highlight the similarities and differences between the Greenland (rigid-bed dominated) and the soft-bed model, in particular the rapid access of stored water in the soft-bed model allowing speed-up events throughout the year, which need to be considered in ice sheet models of glacier response to climate change.

Results

Field site

The study was undertaken at Skálafellsjökull, Iceland (Figure 1a), an outlet glacier of the Vatnajökull Ice Cap which rests on Upper Tertiary grey basalts. This glacier has an area of approximately 100 km^2 and is 25 km in length[36]. The study site was located on the glacier at an elevation of 792 m a.s.l., where the ice was flat and crevasse free. The subglacial meltwater in this area emerges 3 km away at the southern part of the glacier (Staðará river). The glacier is resting on fine grain till (mean grain size 53 µm), with evidence of subglacial deformation in the foreland, with flutes and push moraines[37, 38].

Repeated Ground Penetrating Radar (GPR) surveys (combined with measured glacier depth, video recordings and borehole sampling) have shown that the glacier is resting on a till base (at least 1 m in depth) and the majority of the glacier has a mean radar velocity of 0.177+/- 0.005 m ns^{-1} (water content 0-0.5%) with a thin 1 m debris-rich basal ice layer with a radar velocity of 0.158 +/- 0.003 m ns^{-1} (water content 2%)[37, 39]. From this it was shown that the glacier has little englacial storage, the ice is impermeable and drainage pathways are concentrated in fractures and moulins. Some small till-based cavities were observed with a borehole camera in two of the twenty holes drilled to the glacier base[37]. The bed comprised

three different components: water bodies cover approximately 6% of the area of the bed; a saturated deforming till bed covers 84%; and the remaining 10% comprises an undeforming bed (bedrock, frozen till, low porosity till, lake sediments, outwash sand and gravels)[37, 39]. It was shown that water bodies, during the summer, comprise a series of braided channels with a typical width of 0.5-15 m, mean 3 m, with the velocity from one channel measured at > 0.1 m s^{-1} with a depth of 2 m[37].

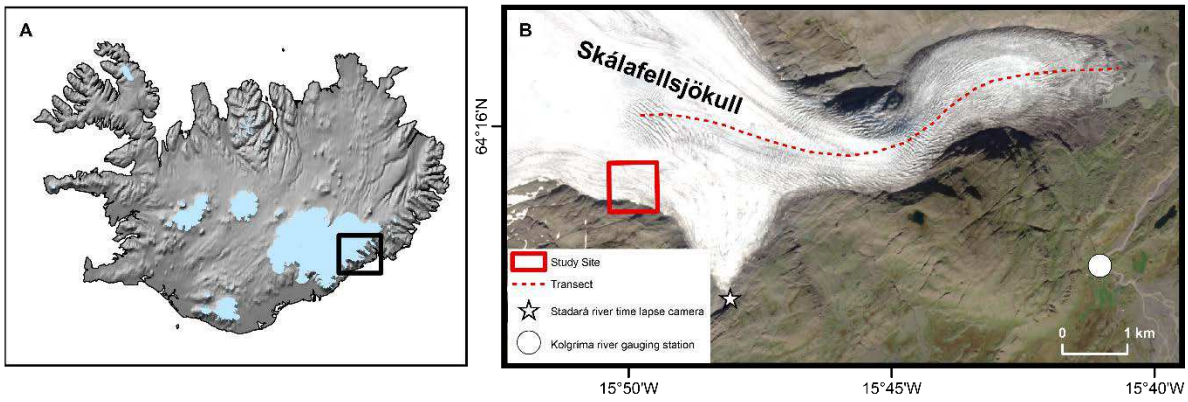

Figure 1*. The field site; a) location within Iceland b) detail of Skálafellsjökull (field site shown with a box). Discharge measurement sites are shown; Staðará river time lapse camera (star) and Kolgríma river gauging station V520 (circle).*

Field data were collected between summer 2008 and autumn 2014, with a continuous discharge record 01/01/2008 – 31/08/2010 and remote sensed imagery between 06/06/2017-24/09/2019. Field data was collected via the Glacsweb environmental sensor network[28, 40, 41] which comprised *in situ* sensor nodes (probes) in the till, base stations and a sensor network server in the UK, as well as GPS and discharge measurements. The Glacsweb probes (0.16 m long) contained micro-sensors measuring water pressure, probe deformation, resistance, tilt and probe temperature. Eight probes, three in the ice and five in the till, sent back between 74 and 397 days of data (details of sensors, readings, locations and errors[41]). Here we discuss the water pressure results, measured in meters water equivalent (m W.E.) (hydraulic head) and expressed as a percentage of glacier thickness (mW.E./h%) from two probes in the till, probe 21 (autumn and winter 2009/10) and probe 25 (summer 2010). Details of the data collection

112 are outlined in the Methods, some of which have discontinuous records due to logistical
113 problems with field data collection including power, connectivity, equipment availability and
114 light levels.

115 **Seasonal patterns**

116 We define the seasons based on the melt rate[42] and identify the winter as the time when there
117 is no melt (apart from a series of warmer days when temperatures rise above zero, which are
118 known as positive degree days), and the melt season as the time when melting occurs. The
119 melt season is divided into three sub-seasons; spring is a time of low melt (where the majority
120 of days are less than the 10% of melt season melt); summer is marked by a high melt; and
121 autumn reflects a distinctly lower level of melt (less than 33% of the melt season melt level)
122 usually with air temperatures falling below zero at night (Figure 2).

123 We show three long-term records reflecting the most extensive data sets. In 2009/10 we
124 collected *in situ* till water pressure (with the wireless Glacsweb probes) and discharge and
125 melt (Figure 2a); in 2012-14 we have surface GPS velocity, discharge and melt (Figure 2b)
126 and in 2017/18 we have remotely sensed velocity and *in-situ* melt data (Figure 2c).

127 Where discharge data is available, we are able to show the relative inputs (mean daily melt)
128 and outputs (mean daily discharge) for each season (Figure 3a). Although there are some
129 annual variations, the general pattern for each season is similar. During the spring, mean
130 daily discharge is relatively similar to the average daily melt (mean discharge 76% of melt).
131 During the summer, mean daily discharge only accounts for 50% of the mean daily melt. In
132 winter, mean daily discharge far exceeds mean daily melt (mean 475%). In autumn, there is
133 interannual variation with melt and discharge at times similar, but mostly the discharge is
134 greater (mean discharge accounts for 100% of melt). There was also variation in the annual
135 patterns of relative melt and discharge (Figure 3b).

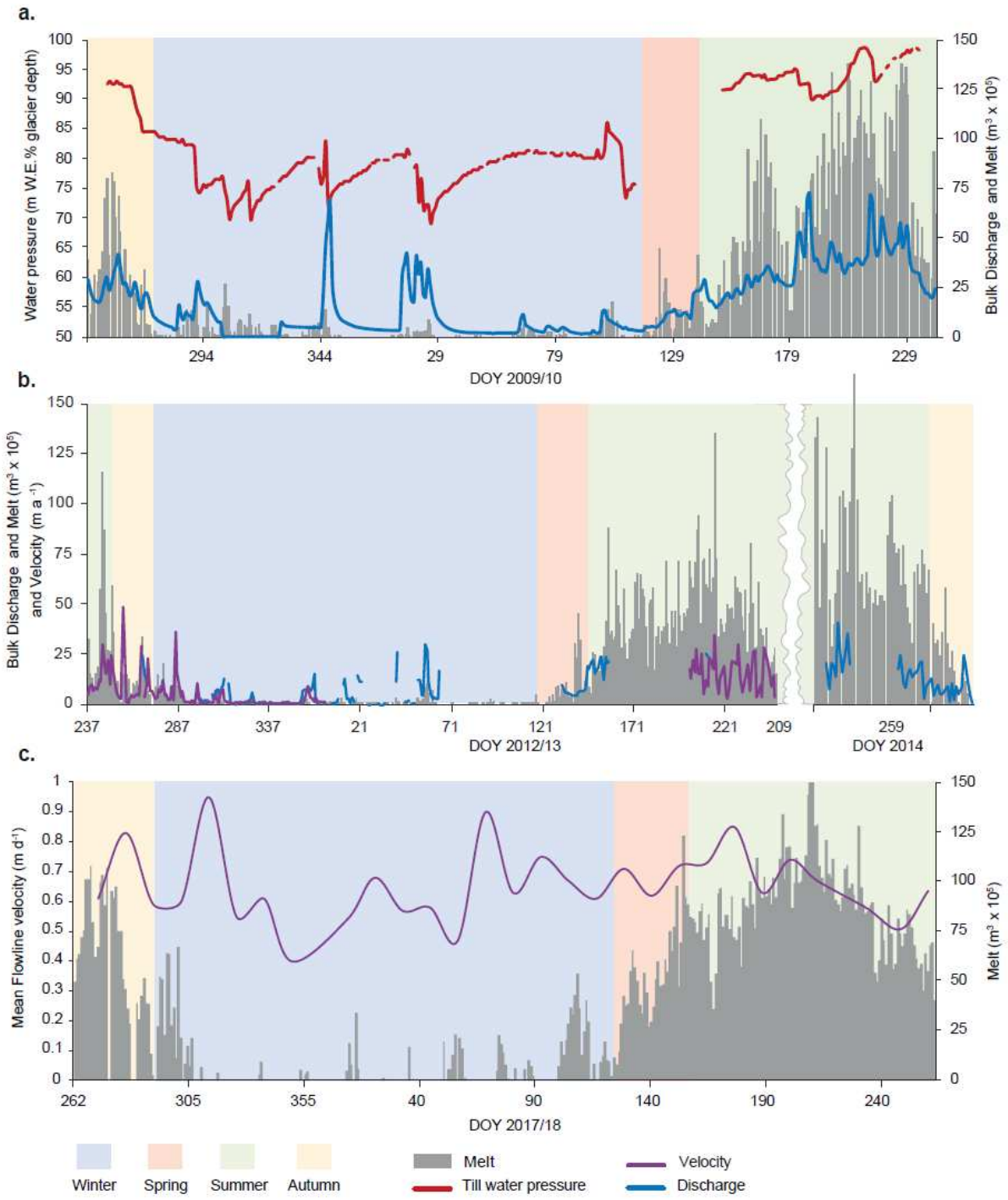

Figure 2. *Long-term records: a) Till water pressure, discharge (Kolgríma river) and melt; b) Ice surface velocity (this data is the scaled average surface velocity from 4 GPS stations to remove local variations), discharge (Staðará river) and melt - 2009/10; c) Mean velocity along the flowline (Sentinal-1 Remote sensed data) and melt 2017/18.*

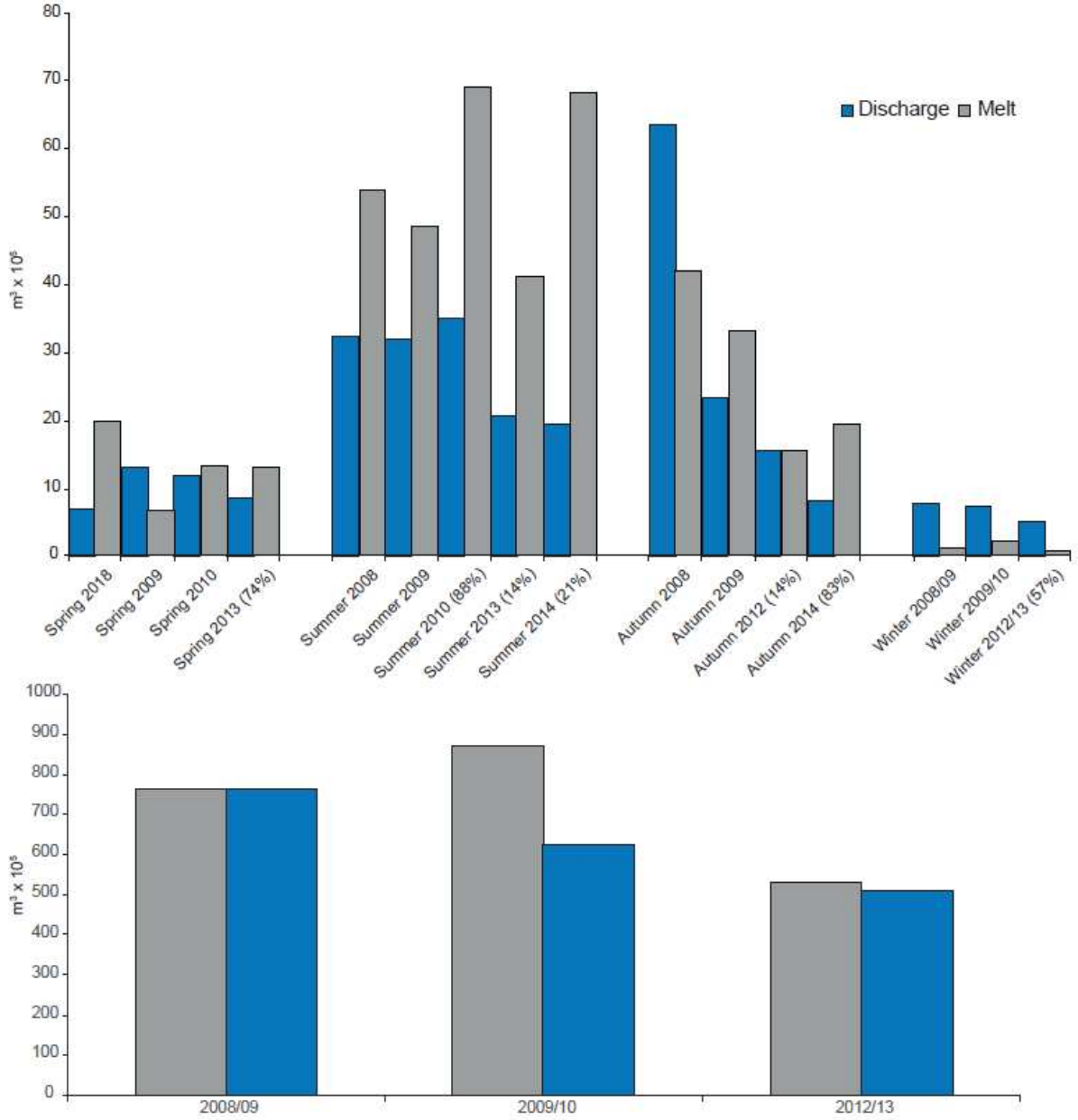

Figure 3. *Relative melt and bulk discharge: a) mean daily melt and discharge per season (where a full record for discharge was not available, the percentage days of the record are shown); b) annual melt and discharge (year begins in autumn).*

Autumn

At the beginning of autumn water pressures in the till are high (2009), but then begin to fall as the melt level decreases (Figure 2a, 2009 DOY 263). The discharge mirrors the melt over the season, and on a diurnal scale, air temperatures and discharge tend to peak at midday and decline overnight.

Autumn has the highest peak velocities (defined as 98% percentile) but the mean daily velocity is less than summer (2012 and 2013 data - autumn = 9.4 m a^{-1}, summer = 12.0 m a^{-1}). The peak velocities coincide with the high melt events (Figure 2b).

Winter

During the winter, daily average temperatures drop below zero so there is little melting on the glacier surface, apart from a series of 'warm' days observed as positive temperatures at the base station and high surface melt. Days with high melt are marked by a small sharp rise and then a dramatic drop in till water pressure (mean 1.77 mW.E./h% per hour, over a 5 hour period), followed by a slow rise in water pressure until the next event. At the same time, discharge dramatically increased as melt increased, normally reaching a peak one day after the melt peak, with continued high discharge for 4-6 days afterwards (Figure 2b).

When temperatures were below zero there was a low base velocity with relatively high peaks during positive degree days (Figure 2b). During the speed-up events, glacier surface horizontal velocities were up to 500% faster than the base level winter horizontal velocity, and lasted between 1-4 days. At the same time there was vertical uplift of the glacier (bed separation), and an increase in discharge (outlined below).

The relationship between the different parameters is shown for one cycle from 2012 DOY 329-362 (Figure 4) (reconstructed data for till water pressure, based on the 2009/10 results have been added for comparison). Each cycle consists of the following phases: Phase I) low or little melt (air temperature below zero) for 3-25 days, associated with low discharge, a base winter velocity, rising till water pressure; Phase II) melt event, causing an increase in discharge, bed separation and surface horizontal velocity, sharp rise and then fall in till water pressure; Phase III) temperatures return to below zero, so melt returns to a low level and velocity returns to a base level, however the discharge remains high for several days, till

water pressures start to rise; Phase IV) discharge falls for one day to an intermediate level before returning to Phase I conditions. Specific details if the 2012/13 cycles are shown in Table 1.

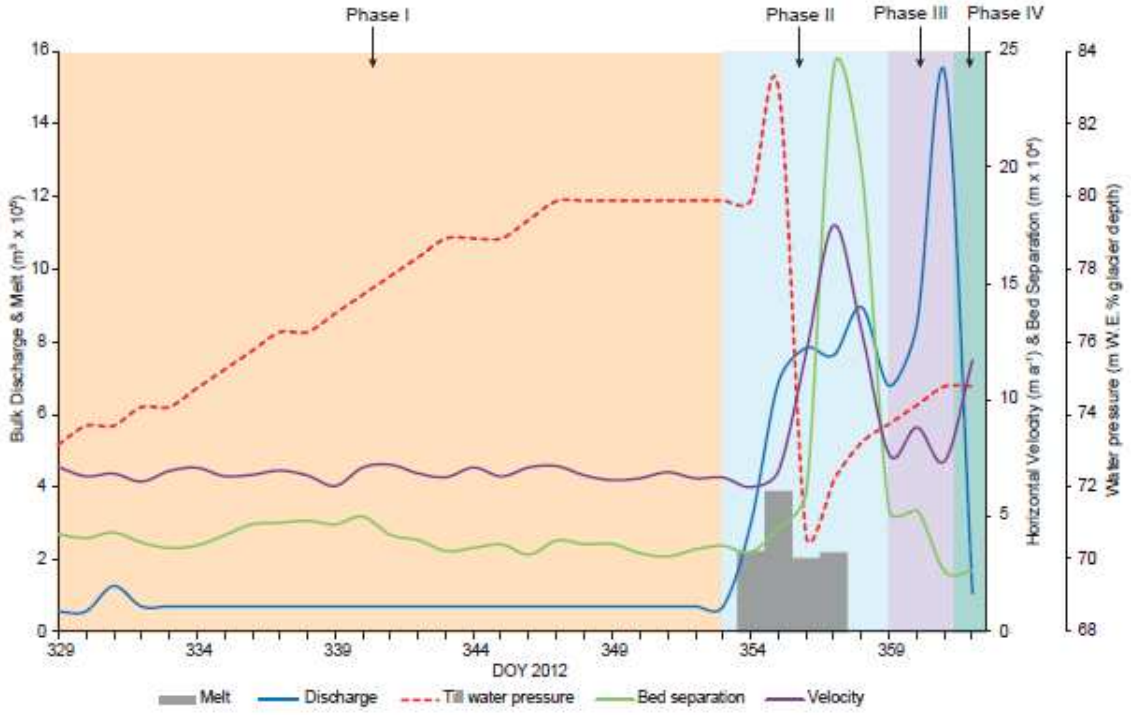

Figure 4*. Detail of cycle 3 (2012) with the different phases shown.*

In order to understand the relationship between melt, storage and discharge we modelled the behavior using a simulation of discharge, which is discussed in the Methods, using the parameters derived from Table 1. The measured discharge and simulation model are very similar with a root mean squared error of 0.84. From this model we can estimate the relative components of the winter discharge: i) 14% is from surface melt; ii) 10% comes from the heat generated from movement and englacial flow (this is discharge minus melt during phase I); iii) 76% is from the melt-event driven subglacial storage release (discharge minus melt during phases II-IV). This shows that the melt driven events are not a minor phenomenon, but a major part of the subglacial hydrology.

188 **Table 1.** Properties of the discharge cycles during winter 2012/13

Cycle number	DOY	Phase I Days with low/no melt			Phase II Days with high melt			Phase III Days with low melt but high discharge		Phase IV Low melt, intermediate discharge	
		Number	Mean melt (m^3)	Mean bulk discharge (m^3)	Number	Threshold melt (m^3)	Bulk discharge (m^3)	Number	Max bulk discharge (m^3) /mean discharge	Number	Bulk discharge at end of cycle (m^3)
1	298-315	11	950	36179	1	17029	73061	4	127735 /110423	1	11151
2	316-328	3	1659	4822	1	14556	13384	7	58048 /16114	1	13568
3	329-362	24	20	4749	4	22519	78272	4	154084 /92297	1	47667
4	363-14	9	5027	6306	3	25108	29276	3	130601 /86074	1	26732
5	15-22	3	4642	18091	1	31195	-	3	144386 /125719	1	-
6	23-43	16	540	1729	2	33899	118169	1	24330	1	-
7	43-61	7	2365	12611	10	32590	120129	-	-	1	33568
Mean (s.d.)	**18.6** (9.8)	**11** (9.0)	**2378** (2323)	**7139** (6344)	**2** (1.4)	**25455** (7612)	**59775** (47730)	**3.6** (2.2)	**118549** (68852)	**1**	**29322** (17196)

189

190 **Spring**

191 The discharge data for spring 2008, 2009, 2010 (diurnal data) and 2013 (4 hourly data) show
192 a similar pattern (Figure 2a, 5a & 5b). There is a slow rise in discharge during early spring
193 (mean 16.75 days) with a small diurnal rise each day around midday. This is followed by a
194 dramatic rise in discharge (over 1-2 days) representing 111% increase in 2008, 68% increase
195 in 2009, 126% increase in 2010). In 2013 this occurred between 13.00 and 17.00 (Figure 5b)

196 with no significant change in air temperature (diurnal increase of 162%). This rapid rise in
197 discharge does not appear to correlate with any specific high melt/temperature event. Once
198 the rise in discharge occurred, flow was consistently high (even at night) and continued to
199 increase even though temperatures were falling (mean 3.5 days). Afterwards the trend in
200 temperatures and discharge were similar and a diurnal pattern returned. We suggest the
201 dramatic rise in discharge marks the spring event, and the return to a positive relationship
202 between air temperature and discharge with a diurnal pattern indicates the beginning of
203 summer. There is also a strong relationship between the date of the beginning of spring and
204 the date of the spring event (r^2 =0.99).

205 We can also investigate how the velocity changes over the spring from the velocity patterns
206 for 2018 and 2019 (Figures 3c, 5c & d). We have shown above that the spring event cannot
207 be identified by the melt/temperature pattern alone, however because we have determined a
208 relationship between the beginning of spring and the spring event, we can predict the date. In
209 2018 this would be approximately DOY 148 and in 2019 DOY 157.

210 In both 2018 and 2019 the early spring velocities were quite similar to peak winter velocities.
211 The spring event can be identified by a distinct rise in velocity close to the predicted date,
212 with an increase in velocity of 16% in 2018 and 35% in 2019. The magnitude of the spring
213 event (in both years) was in the upper part of a range when compared with the peak winter
214 velocities (5.5% above the mean and in the 70% percentile in 2018, 20% above the mean and
215 in the 85% percentile in 2019).

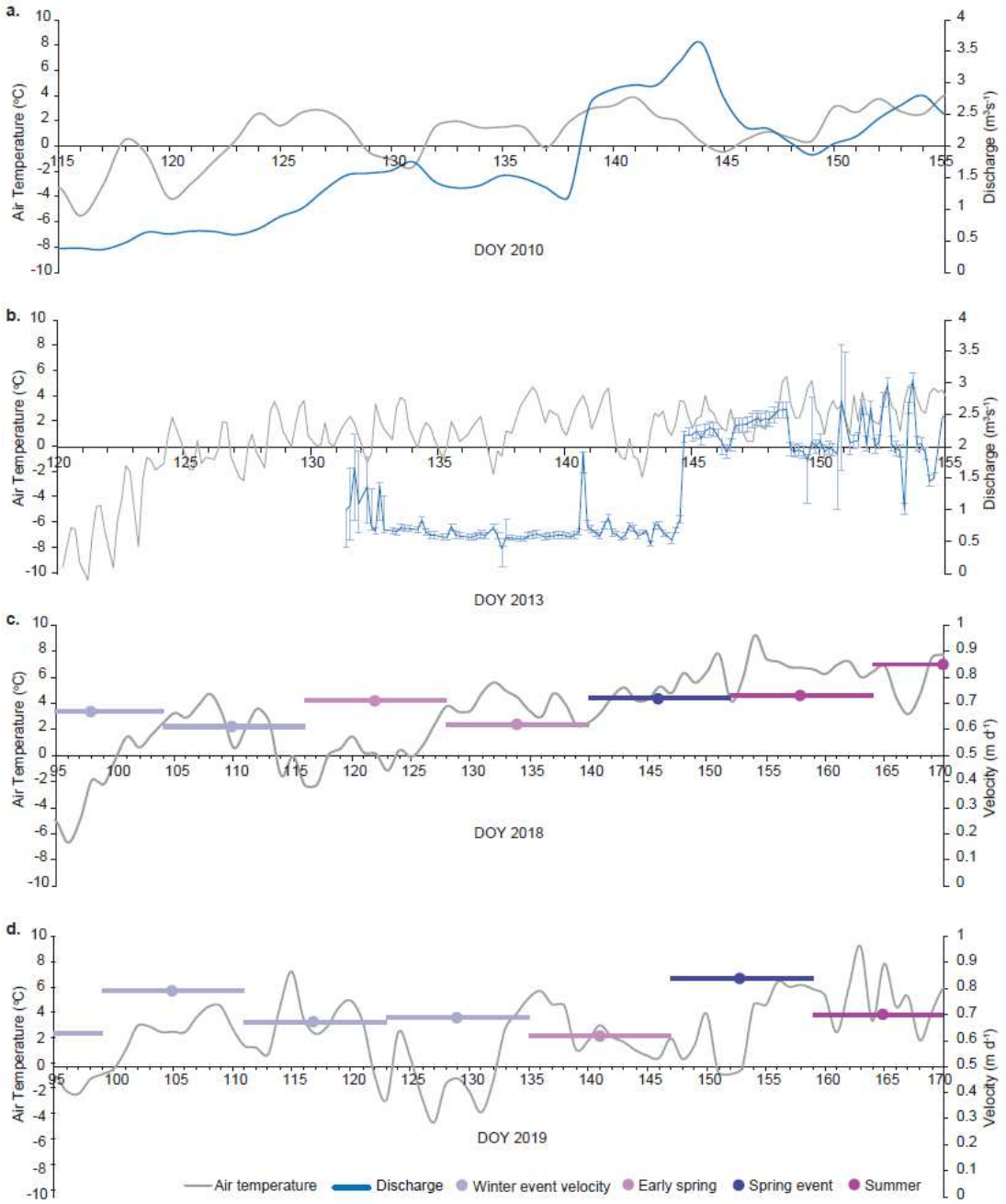

Figure 5. *Spring changes against air temperature: a) Daily discharge during 2010. Spring begins DOY 123, Spring event DOY 139, summer begins DOY 145; b) 4 hourly discharge during 2013, Spring begins DOY 128, Spring event DOY 144, summer begins DOY 148; c) 12 day velocity windows 2018. Spring begins DOY 128, Spring event approx. DOY 143, summer begins DOY 149; d) 12 day velocity windows 2019. Spring begins DOY 133, Spring event approx. DOY 148, summer begins DOY 154.*

Summer

Summer is characterized by high melt, discharge, velocity and water pressure (Figure 2). The twelve day velocity data was compared with the twelve day mean air temperature for the same periods for summer 2017-2019, as well as the average discharge for eight equal periods during the summers of 2008 to 2010 (Figure 6).

Each summer can divided in two parts. The early part of the summer (2010 DOY 144-181) has relatively constant till water pressure, with a positive relationship between melt and discharge (r^2= 0.66). This period is characterized by a low discharge, with the highest velocities (2018 DOY 170) increasing by 28% above the summer mean, and by 18% above the velocities observed during the Spring event

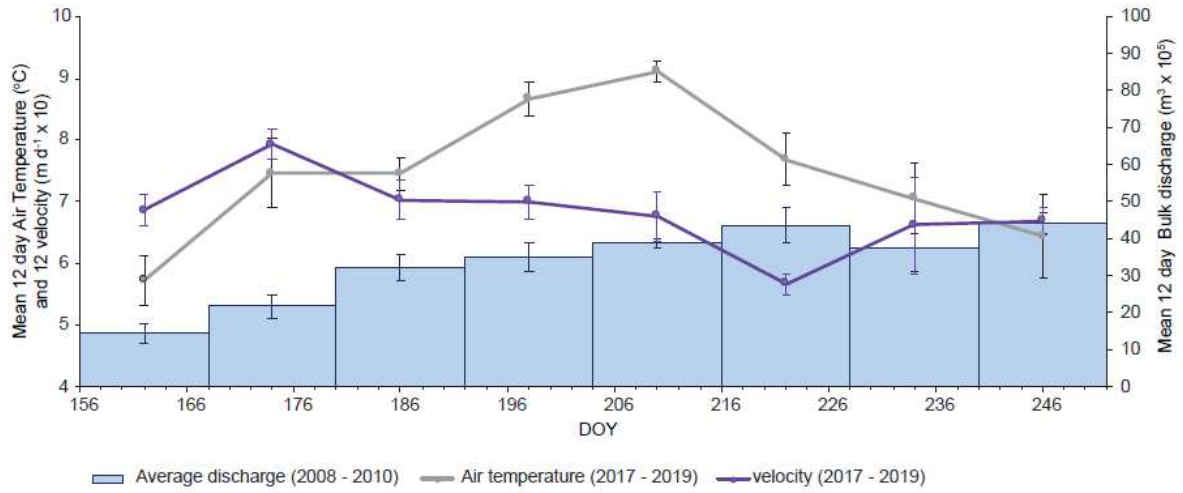

Figure 6. *Mean twelve day summer velocity data against twelve day daily mean air temperatures for summer 2017-19, and mean 12 day discharges for summer 2008-2010.*

During middle to late summer (2010 DOY 182-257) there is change to higher melt and discharge, but no direct relationship between melt and discharge (r^2 =0.11). The discharge is much higher, and in 2010 there were six large discharge events (DOY 184, 189, 199, 215 221, 227-230). Three of these discharge events also showed till water pressure changes. The first two water pressure events were associated with increases in melt water (DOY 182, 187)

242 with immediate decreases in water pressure, followed by a rise in discharge two days later,
243 and a slow increase in till water pressure until the next event. The third event (DOY 213)
244 followed a similar pattern but was not related to any particularly high melt event, rather
245 cumulative high melt over the summer. We assume these abrupt water pressure decreases
246 associated with discharge events are also accompanied by speed-up events (but we have no
247 velocity data for this period). During the summers of 2008 and 2009 there was a similar
248 pattern of discharge peaks occurring after some, but not all of the large melt events.

249 The twelve day velocity data showed the velocities were lower during middle and late
250 summer even though this was the time of highest air temperatures, with a small rise in
251 velocity towards the end of summer (Figure 7). Daily surface velocity data from middle and
252 late summer (2012 DOY 214 – 252, 2013 DOY 200-234) (Figure 2b) showed there was no
253 significant relationship between melt and surface velocity ($r^2 = 0.03$). However the highest
254 and lowest daily velocities tended to coincide with (or occurred the day after) the highest and
255 lowest melt events (Figure 2b).

256 **Annual pattern of change in bulk storage, till water pressure, discharge and velocity.**

257 The data collected from the different years allows us to reconstruct the annual patterns of
258 storage (melt minus discharge, per day[43]), water pressure in the till and velocity over a
259 schematic year (beginning in autumn) (Figure 7). We have used the discharge, melt and till
260 water pressure from 2009/10 and reconstructed the velocity based on the relationships we
261 have determined from the data from other years. The summer is characterized by positive net
262 bulk storage, high till water pressures, with highest mean velocities in early summer, highest
263 melt and discharge in middle and late summer, with melt related speed-up events. Winter is
264 characterized by melt driven events which cause a fall in till water pressure, rise in velocity
265 and negative bulk storage events (evacuation). During autumn there is a decrease in till water

pressure and storage, and very high velocities related to melt. During the spring, the spring event is not related to a specific melt event, but produces a large discharge and velocity rise (similar to the winter high velocities). The storage is generally positive during early spring, and then negative associated with the spring event with a general overall balance.

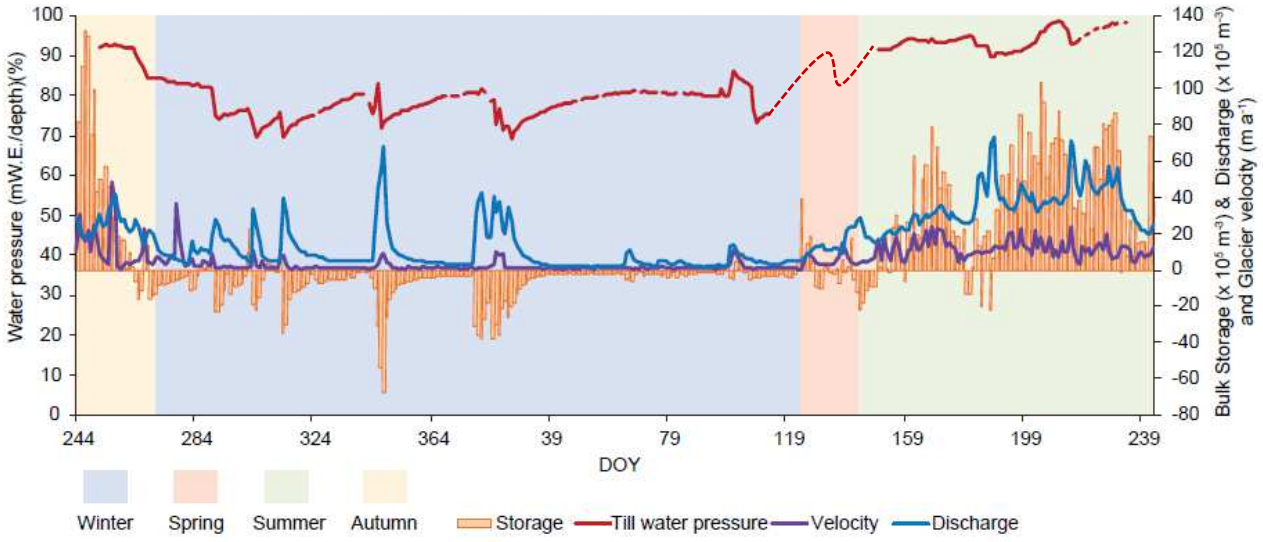

Figure 7*. Composite annual bulk storage (melt minus discharge), till water pressure, melt and discharge from 2009/2010 data, velocity data estimated based on data from other years.*

Over the study period, we can see changes in relative storage (Figure 3b). In 2008/9 and 2012/13 discharge and melt were very similar (99.7% and 96% respectively), but in 2009/10 discharge represented 71% of the melt. Thus the missing water must be stored in the subglacial cavities, debris-rich basal ice[44], subglacial storage and the till and ground water system.

Discussion

There is an emerging picture of soft-bed subglacial hydrology, although much of this is theoretical rather than instrumented. It has been argued[45, 46, 47] that soft-bed subglacial hydrology develops in three stages in response to rising meltwater inputs. At low melt levels water is stored within the till, but once the till becomes saturated, melt water will accumulate

283 at the ice/till interface in a sheet (macroporous layer). At higher melt inputs, rills will form
284 which can grow into shallow streams. Rills typically form anastomosing or braided water
285 courses. It has been suggested that a braided river system was present beneath Storglaciären[22]
286 and that the degree of anastomosing changed with discharge levels throughout the season.
287 Similarity experiments carried out to simulate a pressurized braided subglacial flow under
288 plate glass[48], have shown that as discharge increases the system reorganizes and the degree of
289 braiding intensifies, with a main channel dominant at the highest discharge. As the discharge
290 decreases, water may become isolated from the main channels in unconnected elements
291 ('sloughs' or 'ponds'). This is important as the soft-bed hydrological system beneath West
292 Antarctica have been described as 'swampy'[32, 46], 'distributed'[49] or "water-saturated
293 wetlands"[47]. The latter suggest that the macroporous layer (film) generates a spatially
294 heterogeneous drainage system by eroding the sediment below. It has been reported that
295 beneath Thwaites glacier there is a mixed bed, comprising subglacial highlands (rigid bed
296 dominated) at the margin, with deep channels[50]; and an upstream sedimentary basin (soft-bed
297 dominated) which mostly comprises soft-bed with pooled water[6].

298 We suggest that our data from Skálafellsjökull provides evidence for a soft-bed hydrological
299 system; porous flow within the till (reflected by changing *in situ* till water pressures) and a
300 wide shallow anastomosing system (reported by GPR evidence). Our data provides an
301 instrumented record to corroborate the models discussed above. We now propose how this
302 model can explain seasonal behaviour observed at the site (Figure 8).

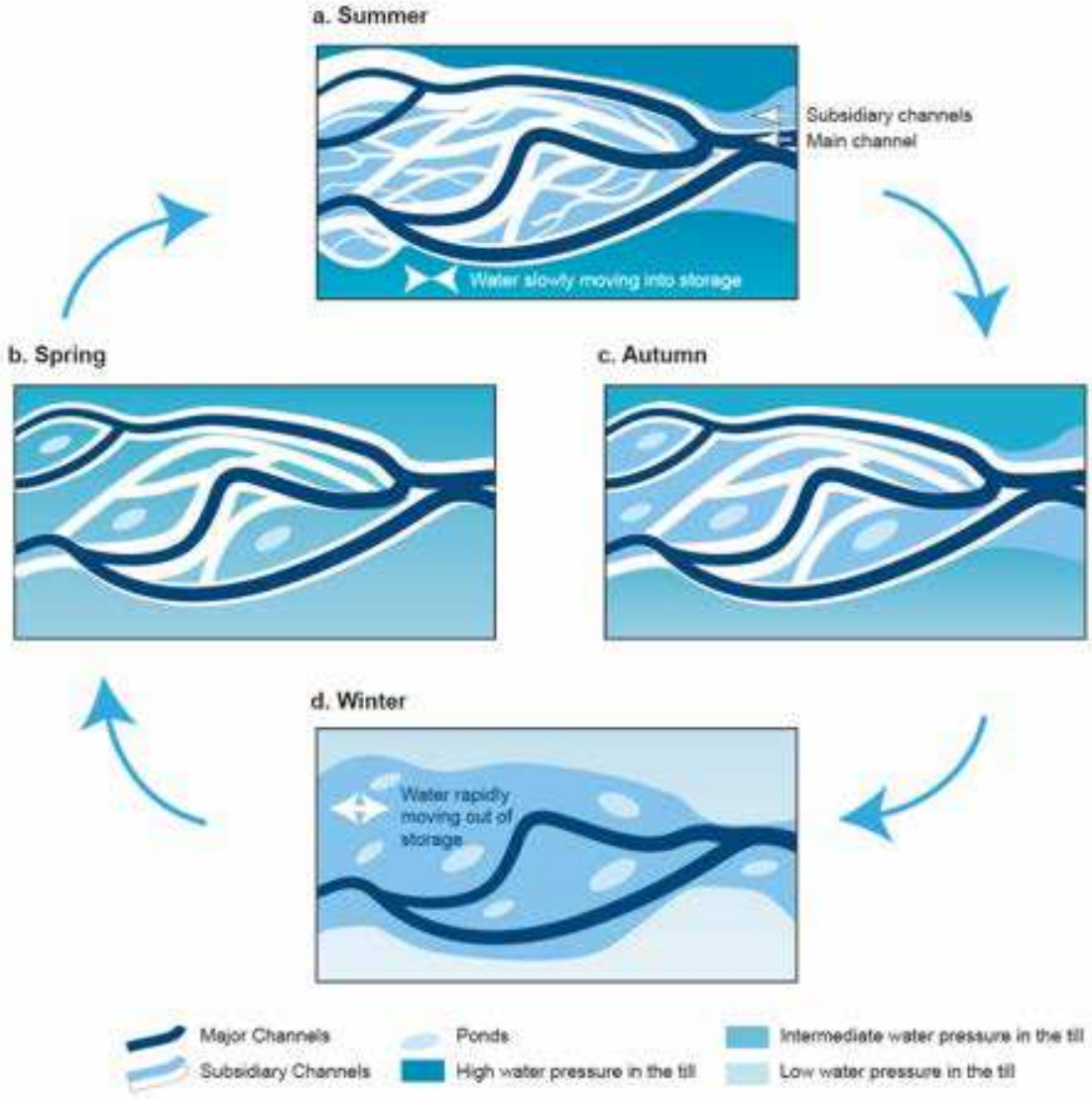

Figure 8. *Model of the seasonal changes associated with anastomosing drainage: a) summer drainage, water is slowly transferred from one storage system to another, b & c) spring and autumn drainage, most water flows in the main channels, is some isolated small reservoirs; d) winter flow, during cold days, slow flow along main channels, during melt events, fast flow of water accessed from storage along a dominant channel.*

During autumn the melt water input gradually reduces and becomes less than the discharge. The level of anastomosing is reduced, and water flow is concentrated along the main channels (Figure 8c). Water may become isolated from the main channels in the unconnected elements and 'ponds' form. At the same time water drains out of the till, which is reflected by the falling water pressures. The water pressures decrease in line with falling melt. We

313 suggest that the highest peak velocities of the year occur at this time because the relatively
314 high melt exceeds the carrying capacity of the subglacial hydrological system, which leads to
315 reduced effective pressure at the bed resulting in speed-up events[51, 52, 53, 43, 8].

316 Winter is characterized by two contrasting behaviours related to surface melt. For most of the
317 winter temperatures are below freezing and there is a low base velocity and low discharge.
318 During positive degree days, surface melt is produced, leading to an increase in glacier
319 surface velocity, bed separation, till water pressure increases for a few hours and then
320 dramatic decline, along with discharge increases (for at least 1-4 days). Then water pressure
321 in the till slowly rises and discharge remains high (4-6 days).

322 We suggest that during the cooler days the subglacial hydrological changes that were begun
323 in autumn continue to develop, i.e. the decrease in the level of anastomosing and the isolation
324 of ponds (Figure 8d). During the melt events, the meltwater quickly drains to the bed where it
325 overwhelms the reduced subglacial hydrological system, which results in a reduction in
326 effective pressure and speed-up accompanied by bed separation and high discharge. The
327 resultant discharge is far greater than the associated meltwater input. To produce the pattern
328 observed, we showed from modelling that during cooler days, the small amount of melt
329 generated by basal friction is added to local storage (cavities or macroporous storage). During
330 the positive degree days, the meltwater itself is released, along with the incremental storage
331 generated from friction since the last melt event, plus an additional element which must come
332 from the longer term (summer) storage.

333 One source is the till, since during bed separation and speed-up, there is a relaxation of the till
334 (associated with stick-slip motion[28]), and water rapidly drains from the till over a very short
335 period (typically less than one day). The second source are the numerous other subglacial
336 reservoirs (cavities, macroporous sources and the ponds) which become ‘connected’ during

bed separation, as water can travel at the ice/till interface into the active channels (Figure 8d). The resultant 'flood' makes a new drainage pattern, which continues until the next melt event. This increased drainage takes four to six days to drain back to the original level and at the same time water drains back into the till and so water pressures rise until the next melt event.

With the onset of spring, the daily melt rate increases, water pressures rise, and the subglacial system supports a relatively stable discharge with a diurnal cycle. We see a dramatic rise in discharge (mean 145% increase) which marks the 'spring event', which is accompanied by a speed-up event[11, 43, 51]. The magnitude of this event was similar to that of the larger winter events, however, unlike the winter events, our 'spring events' were not directly driven by a specific melt event. We suggest that during early spring (approximately 17 days) the increasing melt is accommodated within the main winter channels (Figure 8b). However as the melt increases, it eventually overcomes the system, resulting in the spring event, and in a similar way to the winter melt event, water is released from storage and a new drainage pathway develops. This high discharge continues for 4-5 days draining the new connected areas. After this the discharge pattern reflects surface melt, so we suggest that the new hydrological system is now adapted to the new (higher) summer input level.

Summer is characterized by high levels of water pressure in the till, discharge and surface velocity. We show that in early summer melt and discharge are related, but in late summer there is a more complex pattern. During large discharge events, there is a fall in water pressure. These water pressure/discharge events were not related to absolute melt. The first event (DOY 194, 2010) occurs after a period of low temperatures, and the second (DOY 213, 2010) after a sustained period of high melt. We also show that velocities are highest in early

summer, but are lower in middle and late summer, and velocity peaks are related to melt events.

During summer we suggest that there is an active braided system with both main and subsidiary channels, with the level of anastomosing related to melt. At the beginning of summer, the channels are opening and there is direct flow along the main channels with the beginning of increasing anastomosing as relative melt increases. There is a positive relationship between increased melt, discharge and velocity. However, later in the summer, most increased melt is absorbed by the hydrological system via the increased anastomosing, and so overall velocity decreases (although daily velocities respond to melt). However when inputs exceed the carrying capacity of the system, the storage systems are temporarily overwhelmed, which leads to reduced effective pressure at the bed resulting in speed-up events and water release.

Over the summer as a whole, there is greater input of water to the system than output and so additional daily melt is forced to go into storage; in cavities in the ice, the debris-rich basal ice, the till, the macroporous layer and the braided system itself. Reports of net bulk storage in summer are rare, one study of subglacial storage from Isortoq glacier, Greenland showed that discharge only represented 37-75% of melt season melt[54].

We suggest the following similarities and differences between the 'Greenland' hard-bed dominated and our soft-bed dominated model. Both models show high velocity in early summer resulting from direct melt water imports, with decreasing velocities over late summer as the subglacial hydrology accommodates the water. In Greenland this is due to early summer channelization and late summer increase in a distributed system alongside the channels, comprising linked cavities, with a low hydraulic conductivity covering 66% bed[18, 19]. In the soft-bed example, this is due to increased anastomosing throughout the summer.

This results in high till water pressures and high water storage in the subglacial hydrological system itself (with annual discharge representing 70-100% of annual melt).

Both systems also have speed-up events, when meltwater inputs are higher than the drainage capacity, which results in reduced effective pressure and sliding at the bed. In Greenland this typically happens in spring and autumn[55], whilst at Skálafellsjökull this occurs in all seasons. This is because the soft-bed hydrological system has such high and easily accessible storage capacity, that whenever a speed-up event occurs (particularly in winter) water can be rapidly accessed which has a dramatic effect on the glacier and drainage system.

Methods

Glacsweb Probes

In order to insert probes into the till, boreholes (57 - 69 m deep, approximately 0.1 m diameter) were drilled to the base of the glacier with a Kärcher HDS1000DE jet wash system and the presence of till was examined using a custom made digital infrared LED illuminated colour video camera, via the borehole. If till was present it was hydraulically excavated[56] by maintaining the jet at the bottom of the borehole for an extended period of time. The probes were then lowered into this space, enabling the till to subsequently close in around them. The depth of the probes within the till was approximately 0.1 - 0.2 m beneath the glacier base, estimated from video footage of the till excavation prior to deployment. The probe data were recorded every hour, and transmitted to the base station located on the glacier surface. These data were sent daily via GPRS to a web server in the UK[57].

These water pressure data were calibrated against the measured water depths in the borehole immediately after probe deployment. The glacier thickness (h) was determined from measuring the depth of the boreholes and comparing with the GPS data of the glacier surface.

The probes were designed so that if the data were not immediately accessed then they were stored for later retrieval. There were some problems with communications between the probes and the base station which unfortunately led to the probes filling their programmable memory (EPROM), resulting in some data gaps.

Melt Estimate

Temperature data was measured at the glacier base station (and daily sent back to the UK with the probe data), and also at the Icelandic Meteorological Station at Hofn, 30km away at sea level. The measured lapse rate between the two locations is 0.0082ºC m^{-1}, using data from the 451 days between August 2011 and July 2014 when the base station temperature sensor was not covered with snow. This was used to estimate temperature across the glacier, using the Global ASTER digital elevation model (ASTER GDEM). The altitude of the snow line was estimated from the MODIS daily albedo data (with interpolation where necessary), taking the threshold between ice and snow to be 0.45. Daily melt for the Sultartungnajökull catchment (Figure 1b) was calculated by the degree day algorithm[58, 59], using degree day factors for Satujökull, Iceland: 5.6 mm d^{-1} $ºC^{-1}$ for snow and 7.7 mm d^{-1} $ºC^{-1}$ for ice[60]. All calculations were carried out on the 30m × 30m grid of the ASTER GDEM.

We are able to compare our melt calculations with measured ablation during the field season. Measured mean ablation in 2008 (over a 12 day period from 11 stakes) was 0.036 m d^{-1}, compared with a calculated value of 0.033 m d^{-1} over the same period, and in 2011 the measured mean ablation (over an 11 day period from 15 stakes) was 0.047m d^{-1} compared with the calculated value of 0.044 m d^{-1}.This shows that the calculated ablation depths were 8% lower than the measured results, so although possible sources of error include the degree day factors, albedo and lapse rate, our calculated melt is within an appropriate level of uncertainty with independent field results.

Measurements of Ice velocity

Surface ice velocity was measured from 2008-2012 with a TOPCON Legacy-H L1/L2 GPS (1km baseline) and from 2012-13 with an additional array of 4 dual frequency Leica System 1200 GPS systems at 15 second sampling rate, continuously during the summer and 2 hours a day during the winter (300 m baseline). The GPS data was processed with the ephemeris from the International GPS Service (IGS) stations using TRACK (v. 1.24), the kinematic software package developed by Massachusetts Institute of Technology (MIT) http://geoweb.mit.edu/~tah/track_example/). To account for surface melting, we removed the daily melt from the vertical measurements. The error estimates were as follows (sigma per day): mean North +/- 0.0045m, mean east +/- 0.0032m, mean height +/- 0.0092 m.

The bed separation of the surface ice was calculated using the established Anderson method[28, 61], this methods isolates bed separation from the downward vertical component of mean bed-parallel motion, thinning or thickening of ice associated with ice strain[62] and any till volume changes[63] (till compressibility was assumed to be 10^{-8} Pa^{-1}).

We also calculated surface velocity from Sentinel-1 SAR imagery with a 12 day repeat cycle to show how velocity changed over the whole year (2017-2019). Velocity data was generated using the intensity tracking algorithm within the European Space Agency (ESA) Sentinel Application Platform (SNAP). Intensity tracking is less precise than interferometry but given the high temporal correlation of glacier surfaces, is much more robust[64, 65]. Each pair of SAR images were calibrated and co-registered together using a Digital Elevation Model (DEM)-assisted co-registration based on an airborne LiDAR DEM provided at 5 m resolution from the Icelandic National Land Survey. Velocities were then calculated using cross-correlation with a 5x5 moving window and a search distance of 64 pixels. Any displacements that had a cross-correlation threshold of 0.01 were removed, and the displacements were averaged to a 5

x 5 mean grid and converted to ground range resulting in velocity rasters at 10 m resolution. The stochastic error in our velocity measurements was assessed by measuring displacements over terrain that we regarded as stable[66, 67]. Calculated errors for the Sentinel-1 imagery were +/-0.12 m per day. Mean velocities were then calculated along the center line (Figure 1b).

Discharge

We attained two sets of discharge data from different time periods. One from the Icelandic Meteorological Office gauging station V520 providing a mean daily reading which was operational during our study period from 1st January 2008 to 31st August 2010 (Kolgríma river) (Figure 1b).

The second was from the outlet river at the Sultartungnajökull tongue and was collected using a time lapse camera mounted on a bridge (Figure 1b) (Staðará river) (23rd September 2012 to 16th July 2013 and 28th July 2014 - 4th October 2014). The camera was a Brinno TLC100, an inexpensive time-lapse camera designed for unattended outdoor battery-powered operation. It could capture up to 28,000 frames of 1280 x 1024 pixels, and had a fixed field of view of approximately 50º on the diagonal. Five main sequences were recorded: i) at one-minute intervals from 23 to 26 September 2012 (day of year, DOY 267-270) (which was analyzed at 15 minute intervals); ii) at 4-hour intervals from 22 October 2012 (DOY 296) to 6 June 2013 (DOY 157); iii) a single hand held image from the same location (16th July 2013, DOY 197); iv) at 20 minute intervals from 27th July 2014 (DOY 209) to 1st August 2014 (DOY 213); v) 4-hour intervals from 2nd August 2014 (DOY 214) to 4th October 2014 (DOY 277). In all cases, images were missing when the light level was too low for effective capture or mist blocked the scene. For a substantial part of the second sequence, the course of the river was covered with snow. In addition, there was no data collection between July 2013 and July 2014 due to battery failure.

Estimates of discharge were made by fitting a model of the river bed to the boundary of the water surface in each image, using automatically-detected edges with manual supervision[68]. We then applied the Glauckler-Manning equation to the same model (using a roughness coefficient typical of coarse gravel vegetated streams - 0.04[69]), with the estimated flow cross-section, to compute discharge. To overcome the problem of different sampling rates throughout the season (because of different light levels), we resampled the 24 hour data at shorter intervals to produce correction factors which we were able to apply to the data.

Random errors were estimated by using multiple measurements from different parts of the scene, and were used to remove inconsistent discharge estimates from the time series (> 2 s.d.). It is probably likely that peak discharges are underestimated using the Manning equation due to the fact that flow is highly variable and the relative roughness is going to be highly variable as well. This time-lapse camera method has now also been used by other researchers[70].

The quantity and pattern of the two records is very similar which we will discuss below and gives us confidence that the quantitative results achieved by the time-lapse camera are sufficiently accurate.

Discharge Modelling

Using the 2012/2013 data, each cycle is divided into four phases (Figure 4 and Table 1). Since it can be seen that cycle 1 (DOY 298-315) and cycle 7 (DOY 43-61) in 2012/13 are different from the others (discussed in more detail below), so mean and standard deviation values for the winter have been calculated for cycles 2-6.

500 During the first phase (I) there is low melt, and so the second phase (II) begins on the day
501 when the daily melt M_k first exceeds a threshold M_t, set to 17000 m^3, except for cycle 2 when
502 the threshold is 14000 m^3.

503 During the first stage of the first cycle, prior to the melt exceeding M_t, we assume a linear
504 increase in discharge from a base rate:

505 $$Q_j^{(c)} = Q_0 + jI \quad [4]$$

506

507 where $Q_j^{(c)}$ is the discharge for day j of cycle c. Q_0 is a constant set equal to the observed
508 daily discharge at the start of the cycle 1, equal to 28508 m^3, and I is the daily increment
509 equal to 2500 m^3. This reflects the mean melt during Phase I. In subsequent cycles the daily
510 discharge during the first stage is set to a constant 7000 m^3 (based on the mean discharge
511 during Phase I).

512 The second stage begins on day k of the cycle and ends on day e. During this phase the daily
513 discharge is set equal to the previous day's discharge plus the melt for the day. In addition, on
514 day k the total melt since the start of the cycle is discharged, plus in cycles 5 and 6 an
515 additional volume of 17000 m^3. On the day before the end of the cycle a storage element
516 equal to 2500 m3 multiplied by the number of days since the start of the cycle is added, and
517 on the final day of the cycle the discharge is set to 12000 m^3 (based on the minimum
518 discharge during Phase IV). This can be written as:

519

$$Q_k^{(c)} = Q_{k-1}^{(c)} + \sum_{i=1}^{k} M_i$$
$$Q_j^{(c)} = Q_{j-1}^{(c)} + M_j,\ j = k+1 \ldots e-2$$
$$Q_{e-1}^{(c)} = Q_{j-1}^{(c)} + M_j + 2500(e-3)$$
$$Q_e^{(c)} = 12000$$

520

521

522 Exceptions include: a) during the first cycle (DOY 298 to 315) the initial discharge pattern is
523 very high, with an incremental rise in discharge each day, and b) during the fourth cycle
524 (DOY 363-14) there was no storage release element; however this 'missing' water appears to
525 be released during the fifth cycle (DOY 15-22).

526 **Acknowledgments**

527 The authors would like to thank the Glacsweb Iceland 2008/2011 and 2012 teams for help
528 with probe development and data collection. They would also like to thank Matthew Roberts
529 and Óðinn Þórarinsson, Icelandic Meteorological office for help with data queries and we
530 acknowledge The Icelandic Meteorological Office for the delivery of data from the
531 Hydrological database, no. 2017-09-20/01. Thanks also go to Lyn Ertl in the Cartographic
532 Unit for figure preparation.

533 Supporting data can be accessed at Glacsweb.org and from JKH (jhart@soton.ac.uk).

534 This research was funded by EPSRC (EP/C511050/1), Leverhulme (F/00180/AK) and the
535 National Geographic (GEFNE45-12) and the GPR and Leica 1200 GPS units were loaned
536 from the NERC Geophysical Equipment Facility

Author contributions

J.K.H and K.M designed the study. J.K.H carried out the probe, discharge and GPS data analysis. K.M. designed the sensor network system and Glacsweb probes, as well as the software. D.S.Y. calculated the melt and carried out the discharge modelling. N.R.B and B.A.R derived the remotely sensed surface velocity. J.K.H wrote the manuscript with input from all authors.

References

1. Zemp, M., Huss, M., Thibert, E., Eckert, N., McNabb, R., Huber, J., Barandun, M., Machguth, H., Nussbaumer, S.U., Gärtner-Roer, I. & Thomson, L. Global glacier mass changes and their contributions to sea-level rise from 1961 to 2016. *Nature* **568**(7752), 382 (2019).

2. Fountain, A. G. & Walder, J. S. Water flow through temperate glaciers. *Reviews of Geophysics* **36**(3), 299-328 (1998).

3. Boulton, G. S., Dobbie, K. E. & Zatsepin, S. Sediment deformation beneath glaciers and its coupling to the subglacial hydraulic system. *Quaternary International* **86**, 3-28 (2001).

4. Bougamont, M., Christoffersen, P., A L, H., Fitzpatrick, A.A., Doyle, S.H. & Carter, S.P. Sensitive response of the Greenland Ice Sheet to surface melt drainage over a soft bed. *Nature Communications* **5**, 5052 (2014).

5. Ritz, C., Edwards, T. L., Durand, G., Payne, A. J., Peyaud, V. & Hindmarsh, R. C. Potential sea-level rise from Antarctic ice-sheet instability constrained by observations. *Nature* **528**(7580), 115-118 (2015).

559 6. Muto, A., Anandakrishnan, S., Alley, R. B., Horgan, H. J., Parizek, B. R., Koellner, S., ...
560 & Holschuh, N. Relating bed character and subglacial morphology using seismic data
561 from Thwaites Glacier, West Antarctica. *Earth and Planetary Science Letters* **507**, 199-
562 206 (2019).

563 7. Röthlisberger, H. Water pressure in intra-and subglacial channels. *Journal of Glaciology*
564 **11**(62), 177-203 (1972).

565 8. Schoof, C. Ice-sheet acceleration driven by melt supply variability. *Nature* **468**(7325),
566 803 (2010).

567 9. Wright, P.J., Harper, J.T., Humphrey, N.F. & Meierbachtol, T.W. Measured basal water
568 pressure variability of the western Greenland Ice Sheet: Implications for hydraulic
569 potential. *Journal of Geophysical Research: Earth Surface* **121**(6), 1134-1147 (2016).

570 10. Rada, C. & Schoof, C. Channelized, distributed, and disconnected: subglacial drainage
571 under a valley glacier in the Yukon. *Cryosphere* **12**(8) (2018).

572 11. Iken, A., Röthlisberger, H., Flotron, A. & Haeberli, W. The uplift of Unteraargletscher at
573 the beginning of the melt season—a consequence of water storage at the bed? *Journal of*
574 *Glaciology* **29** (101), 28-47(1983).

575 12. Iken, A., Echelmeyer, K., Harrison, W. & Funk, M. Mechanisms of fast flow in
576 Jakobshavns Isbræ, West Greenland: Part I. Measurements of temperature and water level
577 in deep boreholes. *Journal of Glaciology* **39**(131), 15-25 (1993).

578 13. Bartholomew, I., Nienow, P., Sole, A., Mair, D., Cowton, T., Palmer, S. & Wadham, J.
579 Supraglacial forcing of subglacial drainage in the ablation zone of the Greenland ice
580 sheet. *Geophysical Research Letters,* **38**(8) (2011).

14. Zwally, H. J., Abdalati, W., Herring, T., Larson, K., Saba, J. & Steffen, K. Surface melt-induced acceleration of Greenland ice-sheet flow. *Science* **297**(5579), 218-222 (2002).

15. Joughin, I., Das, S. B., King, M. A., Smith, B. E., Howat, I. M. & Moon, T. (2008). Seasonal speedup along the western flank of the Greenland Ice Sheet. *Science* **320**(5877), 781-783.

16. Sundal, A. V., Shepherd, A., Nienow, P., Hanna, E., Palmer, S. & Huybrechts, P. Melt-induced speed-up of Greenland ice sheet offset by efficient subglacial drainage. *Nature* **469**(7331), 521 (2011).

17. Tedstone, A. J., Nienow, P. W., Gourmelen, N., Dehecq, A., Goldberg, D. & Hanna, E. Decadal slowdown of a land-terminating sector of the Greenland Ice Sheet despite warming. *Nature* **526**(7575), 692 (2015).

18. Andrews, L.C., Catania, G.A., Hoffman, M.J., Gulley, J.D., Lüthi, M.P., Ryser, C., Hawley, R.L. & Neumann, T.A. Direct observations of evolving subglacial drainage beneath the Greenland Ice Sheet. *Nature* **514**(7520), 80 (2014).

19. Hoffman, M. J., Andrews, L. C., Price, S. F., Catania, G. A., Neumann, T. A., Lüthi, M. P., Gulley, J., Ryser, C., Hawley, R. L., & Morriss, B. Greenland subglacial drainage evolution regulated by weakly connected regions of the bed. *Nature communications* **7**, 13903 (2016).

20. Downs, J. Z., Johnson, J. V., Harper, J. T., Meierbachtol, T., & Werder, M. A. Dynamic hydraulic conductivity reconciles mismatch between modeled and observed winter subglacial water pressure. *Journal of Geophysical Research: Earth Surface* **123**(4), 818-836 (2018).

603 21. Davison, B.J., Sole, A.J., Livingstone, S.J., Cowton, T.R. & Nienow, P.W. The influence
604 of hydrology on the dynamics of land-terminating sectors of the Greenland Ice Sheet.
605 *Frontiers in Earth Science* **7** (2019).

606 22. Hock, R. & Hooke, R. L. Evolution of the internal drainage system in the lower part of
607 the ablation area of Storglaciären, *Sweden. Geol. Soc. Am. Bull.* **105**, 537–546 (1993).

608 23. Walder, J. S. & Fowler, A. Channelized subglacial drainage over a deformable bed.
609 *Journal of Glaciology* **40**, 3 – 15(1994).

610 24. Creyts, T.T. & Schoof C.G. Drainage through subglacial water sheets. *Journal of*
611 *Geophysical Research: Earth Surface* **114**(F4) (2009).

612 25. Hart, J.K. & Boulton, G.S. The interrelation of glaciotectonic and glaciodepositional
613 processes within the glacial environment. *Quaternary Science Reviews* 10(4), 335-350
614 (1991).

615 26. Iverson, N.R. Shear resistance and continuity of subglacial till: hydrology rules. *Journal*
616 *of Glaciology* **56**(200), 1104-1114 (2010).

617 27. Damsgaard, A., Egholm, D.L., Beem, L.H., Tulaczyk, S., Larsen, N.K., Piotrowski, J.A.
618 & Siegfried, M.R. Ice flow dynamics forced by water pressure variations in subglacial
619 granular beds. *Geophysical Research Letters* **43**(23), doi:10.1002/2016GL071579 (2019).

620 28. Hart, J.K., Martinez, K., Basford, P.J., Clayton, A.I., Bragg, G.M., Ward, T. & Young, D.
621 S. Surface melt-driven seasonal behaviour (englacial and subglacial) from a soft-bedded
622 temperate glacier recorded by in situ wireless probes. *Earth Surface Landforms and*
623 *Processes* https://doi.org/10.1002/esp.4611(2019)

29. Hubbard, B. & Nienow, P. Alpine subglacial hydrology. *Quaternary Science Reviews* **16**(9), 939-955 (1997).

30. Flowers, G.E. Modelling water flow under glaciers and ice sheets. *Proceedings of the Royal Society A: Mathematical, Physical and Engineering Sciences* **471**(2176), p.20140907 (2015).

31. Ng, F.S. Coupled ice–till deformation near subglacial channels and cavities. *Journal of Glaciology* **46**(155), 580-598 (2000).

32. Schroeder, D.M., Blankenship, D.D. & Young, D.A. Evidence for a water system transition beneath Thwaites Glacier, West Antarctica. *P. Natl. Acad. Sci.* **110**, 12225–12228 (2013).

33. Joughin, I., Smith, B.E. & Medley, B. Marine ice sheet collapse potentially under way for the Thwaites Glacier Basin, West Antarctica. *Science* **344**(6185), 735-738 (2014).

34. Kulessa, B., Hubbard, A.L., Booth, A.D., Bougamont, M., Dow, C.F., Doyle, S.H., Christoffersen, P., Lindbäck, K., Pettersson, R., Fitzpatrick, A.A. & Jones, G.A. Seismic evidence for complex sedimentary control of Greenland Ice Sheet flow. *Science advances* **3**(8), 1603071 (2017).

35. DeConto, R.M. & Pollard, D. Contribution of Antarctica to past and future sea-level rise. *Nature* **531**, 591-597 (2016).

36. Hannesdóttir, H., Björnsson, H., Pálsson, F., Aðalgeirsdóttir, G. & Guðmundsson, S. Changes in the southeast Vatnajökull ice cap, Iceland, between~ 1890 and 2010. *The Cryosphere* **9**(2), 565-585 (2015).

645 37. Hart, J.K., Rose, K. C., Clayton, A., & Martinez, K. Englacial and subglacial water flow
646 at Skálafellsjökull, Iceland derived from ground penetrating radar, in situ Glacsweb probe
647 and borehole water level measurements. *Earth Surface Processes and Landforms* **40**(15),
648 2071-2083 (2015).

649 38. Hart, J.K., Martinez, K., Basford, P.J., Clayton, A.I., Robson, B.A. & Young, D. S.
650 Surface melt driven summer diurnal and winter multi-day stick-slip motion and till
651 sedimentology. *Nature Communications* 10.1038/s41467-019-09547-6 (2019a).

652 39. Hart, J.K., Martinez, K., Basford, P.J., Clayton, A.I., Bragg, G.M., Ward, T., & Young,
653 D. S. Surface melt-driven seasonal behaviour (englacial and subglacial) from a soft-
654 bedded temperate glacier recorded by in situ wireless probes. *Earth Surface Landforms*
655 *and Processes* https://doi.org/10.1002/esp.4611 (2019b).

656 40. Hart, J.K. & Martinez, K. Environmental Sensor Networks: A revolution in the earth
657 system science? *Earth-Science Reviews* **78**(3), 177-191 (2006).

658 41. Martinez, K., Hart, J. K., Basford, P. J., Bragg, G. M., Ward, T. & Young D. S. A
659 geophone wireless sensor network for investigating glacier stick-slip motion. *Computers*
660 *and Geoscience* **105**, 103-112 (2017).

661 42. Stevens, L.A., Behn, M.D., Das, S.B., Joughin, I., Noël, B.P., van den Broeke, M.R., &
662 Herring, T., Greenland Ice Sheet flow response to runoff variability. *Geophysical*
663 *Research Letters* **43**(21), 11-295 (2016).

664 43. Bartholomaus, T. C., Anderson, R. S. & Anderson, S. P. Response of glacier basal motion
665 to transient water storage. *Nature Geoscience* **1**(1), 33 (2008).

666 44. Chu, W., Schroeder, D.M., Seroussi, H., Creyts, T.T., Palmer, S.J. & Bell, R.E. Extensive
667 winter subglacial water storage beneath the Greenland Ice Sheet. *Geophysical Research*
668 *Letters* **43**(24) (2016).

669 45. Alley, R.B. Water-pressure coupling of sliding and bed deformation: I. Water system.
670 *Journal of Glaciology* **35**(119), 108-118 (1989).

671 46. Kyrke-Smith, T.M. & Fowler, A.C. Subglacial swamps. *Proceedings of the Royal Society*
672 *A: Mathematical, Physical and Engineering Sciences* **470**(2171), p.20140340 (2014).

673 47. Kasmalkar, I., Mantelli, E. & Suckale, J. Spatial heterogeneity in subglacial drainage
674 driven by till erosion. *Proceedings of the Royal Society A* **475**(2228), p.20190259 (2019).

675 48. Catania, G. & Paola, C. Braiding under glass. *Geology* **29**(3), 259-262 (2001).

676 49. Hodson, T. O., Powell, R. D., Brachfeld, S. A., Tulaczyk, S., Scherer, R. P. & Team, W.
677 S. Physical processes in Subglacial Lake Whillans, West Antarctica: inferences from
678 sediment cores. *Earth and Planetary Science Letters* **444**, 56-63 (2016).

679 50. Hogan, K.A., Larter, R.D., Graham, A.G., Arthern, R., Kirkham, J.D., Totten Minzoni,
680 R., Jordan, T.A., Clark, R., Fitzgerald, V., Wåhlin, A.K. & Anderson, J.B. Revealing the
681 former bed of Thwaites Glacier using sea-floor bathymetry: implications for warm-water
682 routing and bed controls on ice flow and buttressing. *The Cryosphere* **14**(9), 2883-2908
683 (2020).

684 51. Iken, A. & Bindschadler, R. A. Combined measurements of subglacial water pressure and
685 surface velocity of Findelengletscher, Switzerland: conclusions about drainage system
686 and sliding mechanism. *Journal of Glaciology* **32**(110), 101-119(1986),

687 52. Sugiyama, S., & Gudmundsson, G. H. Short-term variations in glacier flow controlled by
688 subglacial water pressure at Lauteraargletscher, Bernese Alps, Switzerland. *Journal of*
689 *Glaciology* **50**(170), 353-362 (2004).

690 53. Nienow, P. W., Hubbard, A. L., Hubbard, B. P., Chandler, D. M., Mair, D. W. F., Sharp,
691 M. J. & Willis, I. C. Hydrological controls on diurnal ice flow variability in valley
692 glaciers. *J. Geophys. Res.* **110**, F04002, doi:10.1029/2003JF000112 (2005).

693 54. Smith, L. C., Chu, V. W., Yang, K., Gleason, C. J., Pitcher, L. H., Rennermalm, A. K. &
694 Tedesco, M. Efficient meltwater drainage through supraglacial streams and rivers on the
695 southwest Greenland ice sheet. *Proceedings of the National Academy of Sciences* **112**(4),
696 1001-1006 (2015).

697 55. Van de Wal, R.S.W., Smeets, C.J.P.P., Boot, W., Stoffelen, M., Van Kampen, R., Doyle,
698 S.H., Wilhelms, F., van den Broeke, M.R., Reijmer, C.H., Oerlemans, J. & Hubbard, A.
699 Self-regulation of ice flow varies across the ablation area in south-west Greenland.
700 *Cryosphere* **9** (2), 603-611 (2015),

701 56. Blake, E.W., Clarke, G.K.C. & Gerrin, M.C. Tools for examining subglacial bed
702 deformation. *Journal of Glaciology* **38**, 388-396 (1992).

703 57. Martinez, K., Hart, J. K. & Ong, R. Deploying a Wireless Sensor Network in Iceland, in
704 *GeoSensor Networks*, GSN 2009, eds. N. Trigoni, Markham A. and Nawaz S., Lecture
705 Notes in Computer Science, vol 5659. (Springer, Berlin, Heidelberg) (2009).

706 58. Braithwaite, R.J. Positive Degree-Day Factors for Ablation on the Greenland Ice-Sheet
707 Studied by Energy-Balance Modelling. *Journal of Glaciology* **41**, 153-160 (1995).

59. Hock, R. Temperature index temperature modelling in mountain areas. *Journal of Hydrology* **282**, 104-115 (2003).

60. Johannesson, T., Sigurdsson, O., Laumann, T. & Kennett, M. Degree-day glacier mass-balance modelling with applications to glaciers in Iceland, Norway and Greenland. *Journal of Glaciology* **41** (138), 345–358 (1995).

61. Anderson, R.S., Anderson, S.P., MacGregor, K.R., Waddington, E.D., O'Neel, S, Riihimaki, C.A. & Loso, M.G. Strong feedbacks between hydrology and sliding of a small alpine glacier. *Journal of Geophysical Research: Earth Surface* **109**(F3) (2004).

62. Hooke, R.L., Calla, P., Holmlund, P., Nilsson, M., & Stroeven, A. A 3 year record of seasonal variations in surface velocity, Storglaciären, Sweden. *Journal of Glaciology* **35**(120), 235-247 (1989).

63. Truffer, M., Echelmeyer, K. A. & Harrison, W. D. Implications of till deformation on glacier dynamics. *Journal of Glaciology* **47**(156), 123-134 (2001).

64. Nagler, T., Rott, H., Hetzenecker, M., Scharrer, K., Magnússon, E., Floricioiu, D., & Notarnicola, C. Retrieval of 3D-glacier movement by high resolution X-band SAR data. In 2012 IEEE International Geoscience and Remote Sensing Symposium (pp. 3233-3236), IEEE (2012, July) (2012),

65. Fahnestock, M., Scambos, T., Moon, T., Gardner, A., Haran, T. & Klinger, M. Rapid large-area mapping of ice flow using Landsat 8. *Remote Sensing of Environment* **185**, 84-94 (2016).

66. Robson, B.A., Nuth, C., Nielsen, P.R., Girod, L., Hendrickx, M. & Dahl, S.O. Spatial variability in patterns of glacier change across the Manaslu Range, Central Himalaya. *Frontiers in Earth Science* **6***,* 1-12 (2018).

67. Baurley, N.R., Robson, B., & Hart, J.K. Long-term impact of the proglacial lake Jökulsárlón on the flow velocity and stability of Breiðamerkurjökull glacier, Iceland. *Earth Surface Processes and Landforms* **45** (11), 2647-2663 (2020).

68. Young, D.S., Hart, J.K. & Martinez, K. Image analysis techniques to estimate river discharge using time-lapse cameras in remote locations. *Computers & Geosciences* **76**, 1-10 (2015).

69. Aldridge, B.N. & Garrett, J.M. Roughness coefficients for stream channels in Arizona (No. 73-3). *US Geological Survey* (1973).

70. Leduc, P., Ashmore, P. & Sjogren, D. Stage and water width measurement of a mountain stream using a simple time-lapse camera. *Hydrology and Earth System Sciences* **22**(1), 1-11 (2018).

Figures

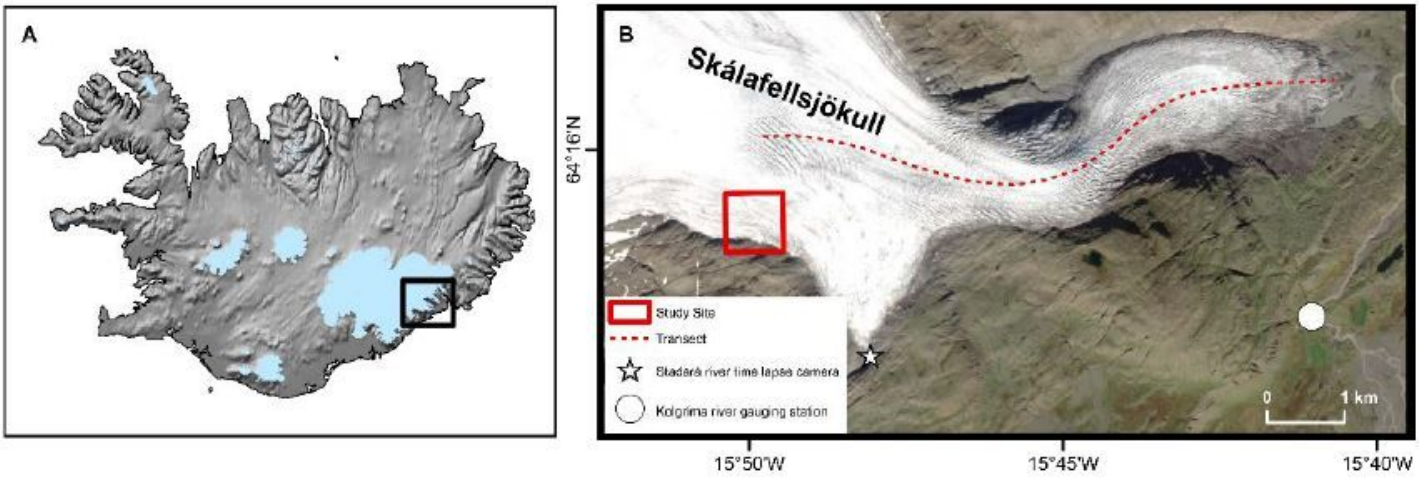

Figure 1

The field site; a) location within Iceland b) detail of Skálafellsjökull (field site shown with a box). Discharge measurement sites are shown; Staðará river time lapse camera (star) and Kolgríma river gauging station V520 (circle). Note: The designations employed and the presentation of the material on this map do not imply the expression of any opinion whatsoever on the part of Research Square concerning the legal status of any country, territory, city or area or of its authorities, or concerning the delimitation of its frontiers or boundaries. This map has been provided by the authors.

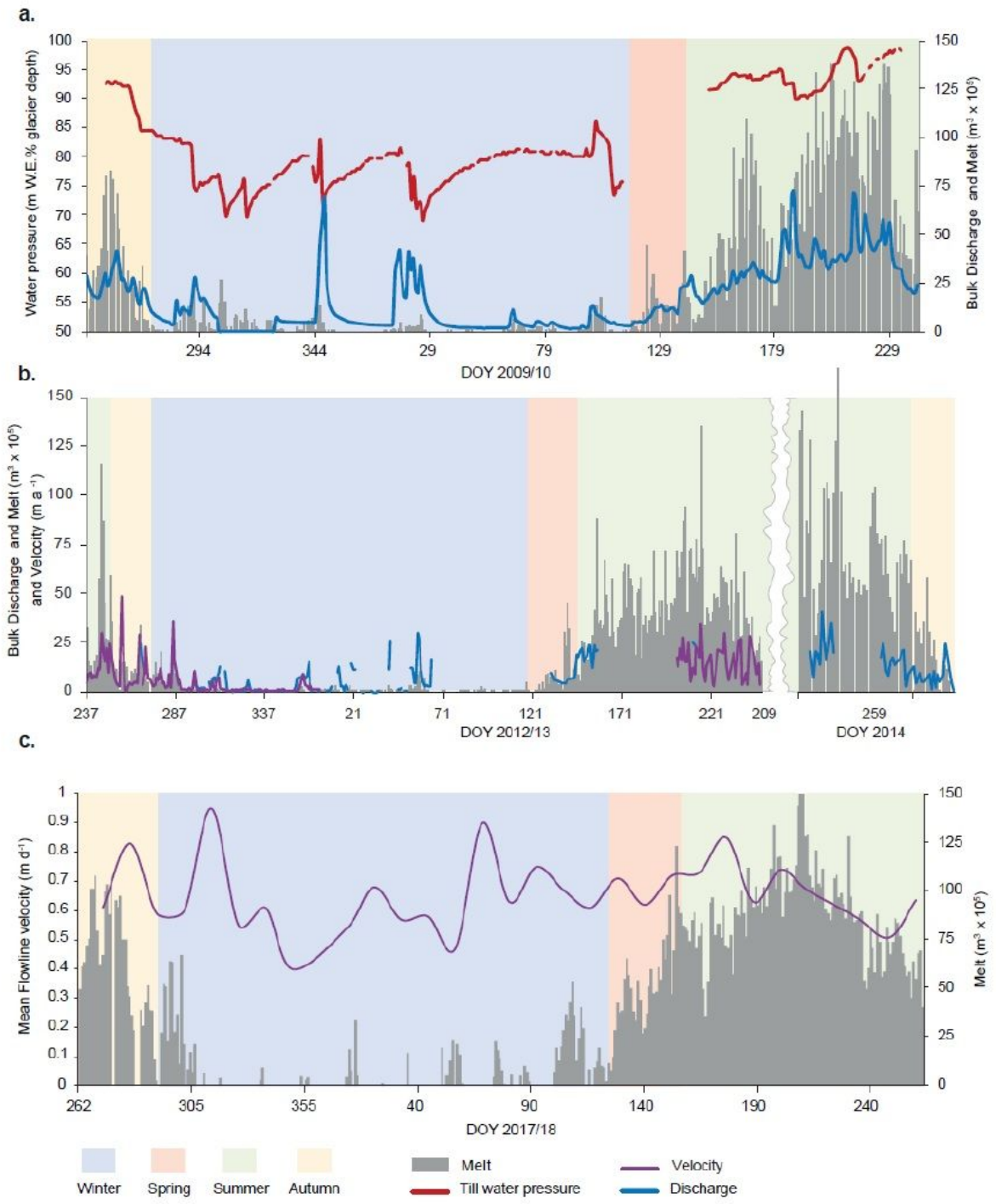

Figure 2

Long-term records: a) Till water pressure, discharge (Kolgríma river) and melt; b) Ice surface velocity (this data is the scaled average surface velocity from 4 GPS stations to remove local variations), discharge (Staðará river) and melt - 2009/10; c) Mean velocity along the flowline (Sentinal-1 Remote sensed data) and melt 2017/18.

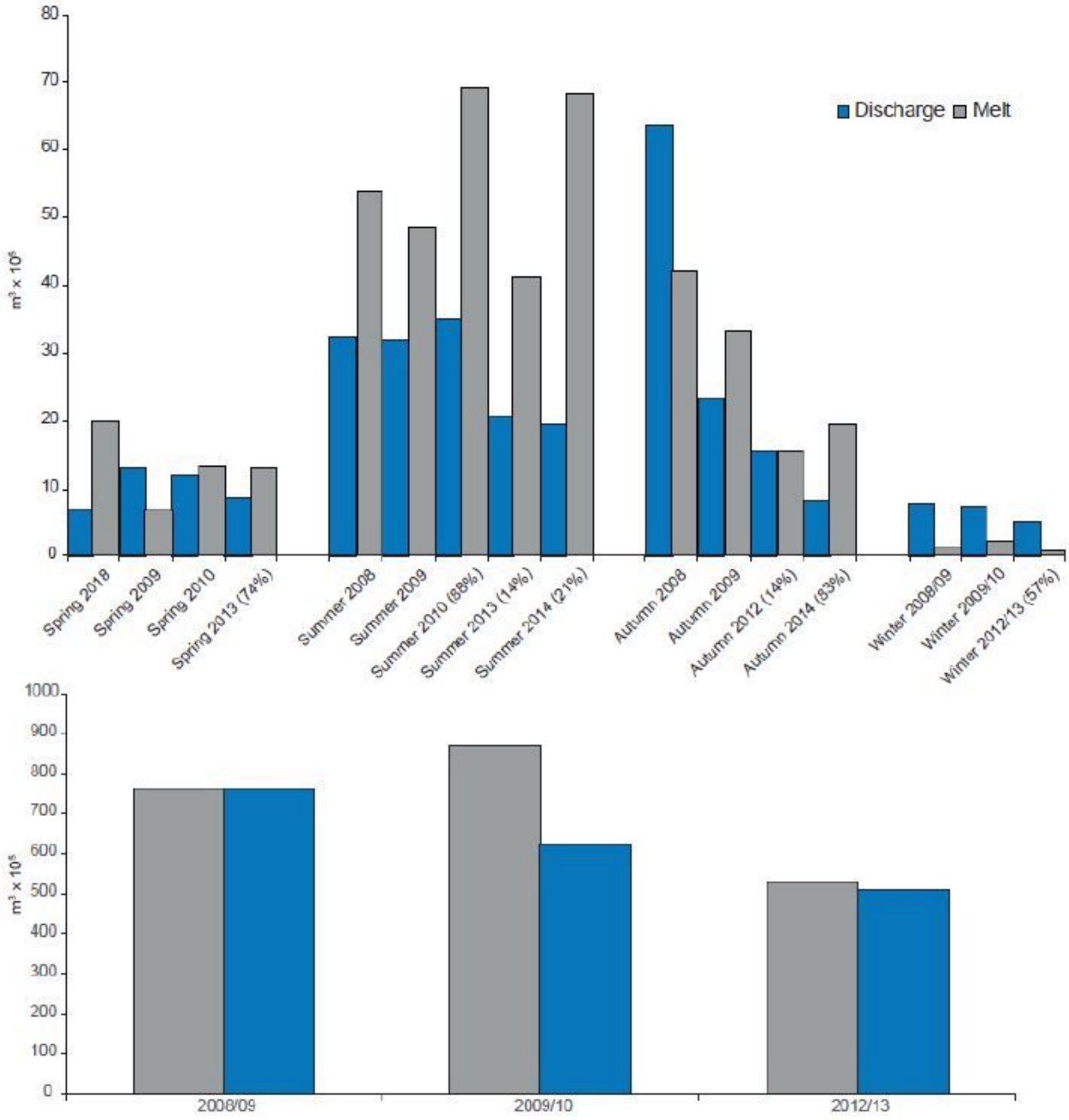

Figure 3

Relative melt and bulk discharge: a) mean daily melt and discharge per season (where a full record for discharge was not available, the percentage days of the record are shown); b) annual melt and discharge (year begins in autumn).

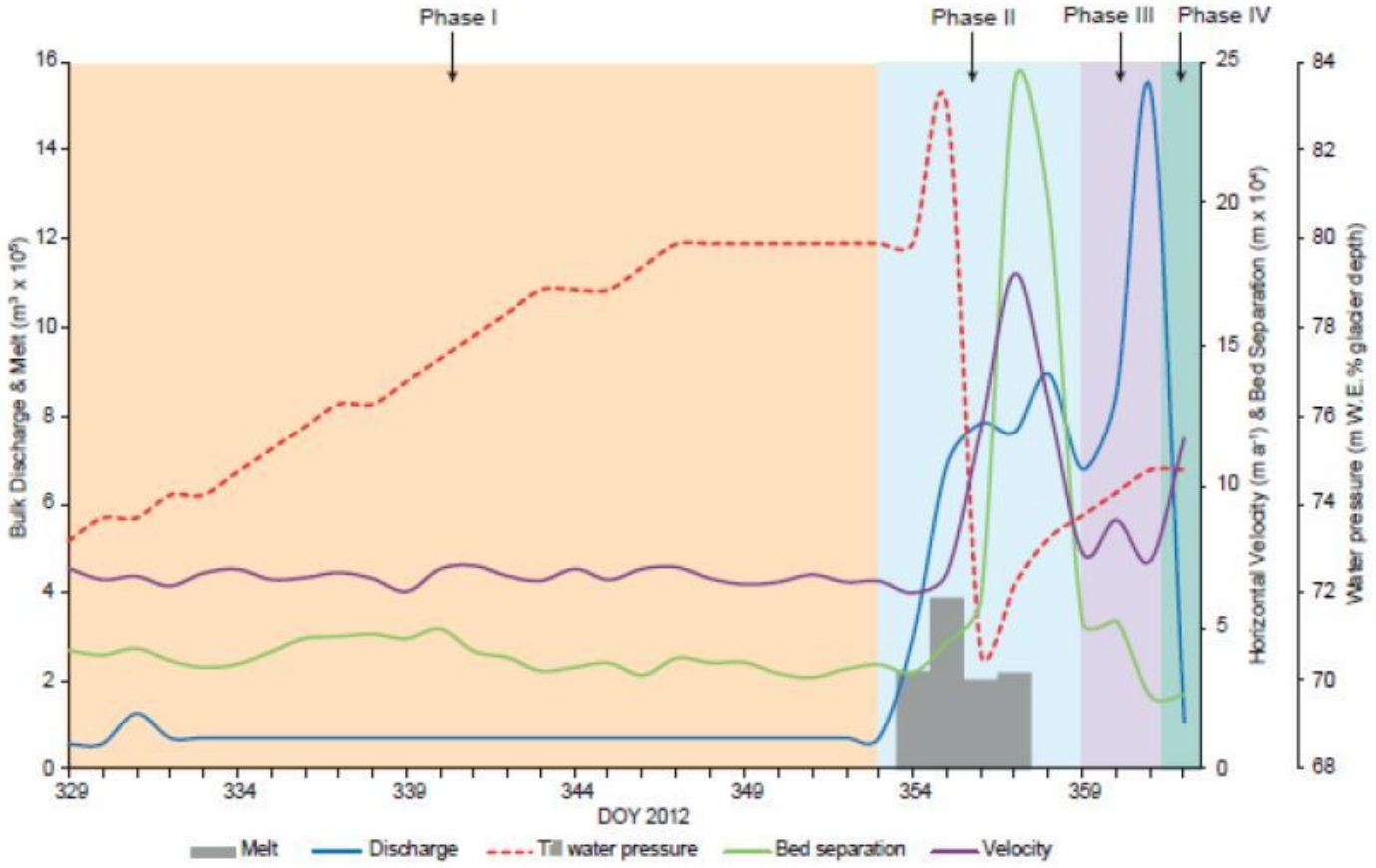

Figure 4

Detail of cycle 3 (2012) with the different phases shown.

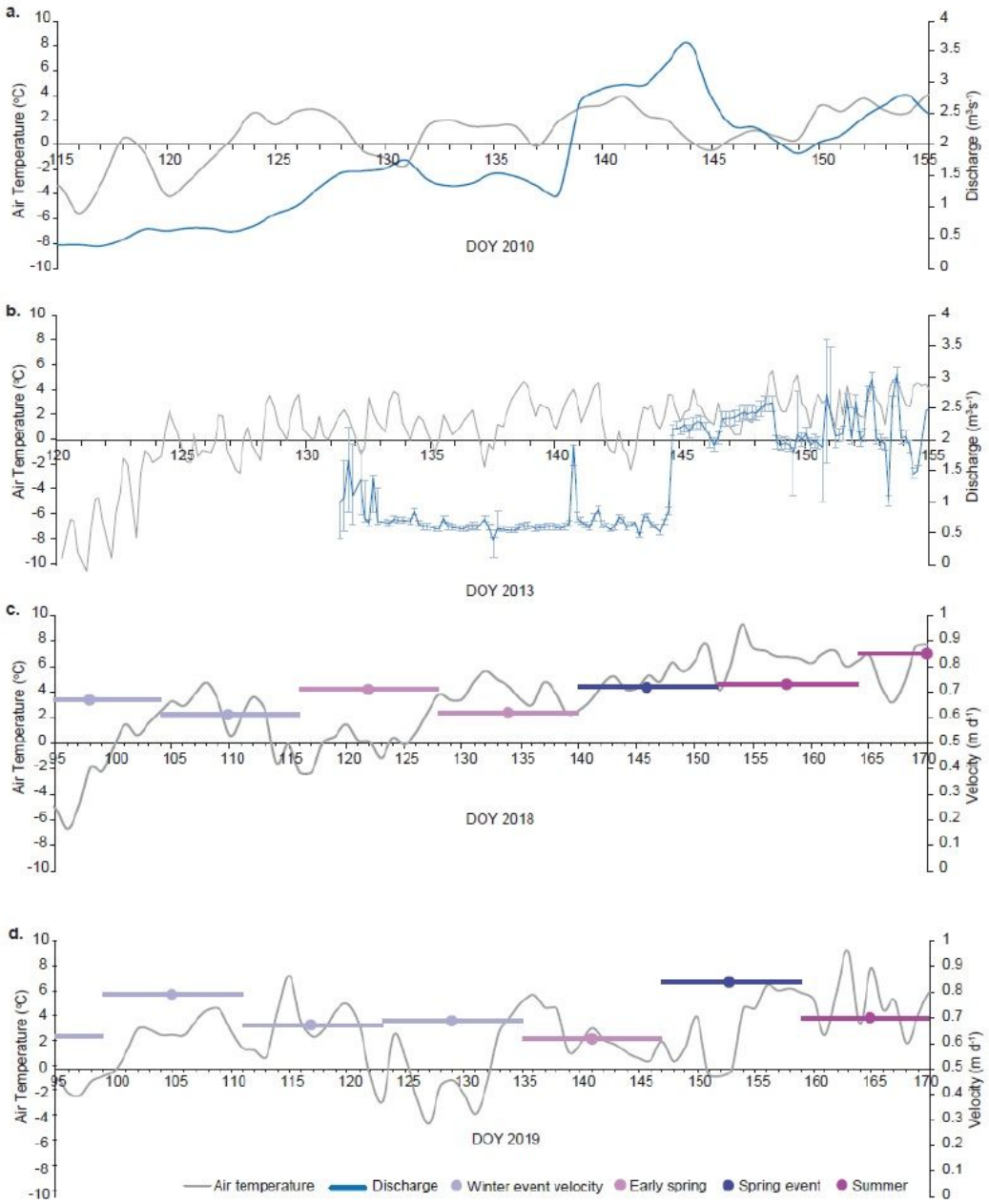

Figure 5

Spring changes against air temperature: a) Daily discharge during 2010. Spring begins DOY 123, Spring event DOY 139, summer begins DOY 145; b) 4 hourly discharge during 2013, Spring begins DOY 128, Spring event DOY 144, summer begins DOY 148; c) 12 day velocity windows 2018. Spring begins DOY 128, Spring event approx. DOY 143, summer begins DOY 149; d) 12 day velocity windows 2019. Spring begins DOY 133, Spring event approx. DOY 148, summer begins DOY 154.

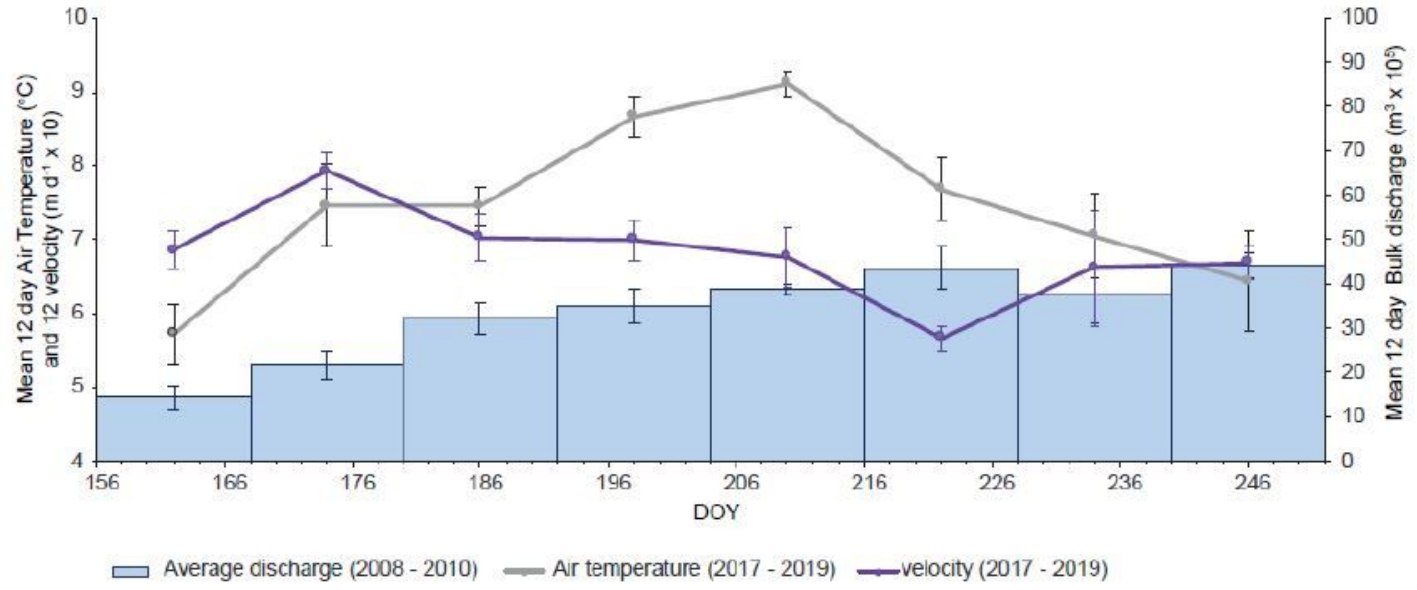

Figure 6

Mean twelve day summer velocity data against twelve day daily mean air temperatures for summer 2017-19, and mean 12 day discharges for summer 2008-2010.

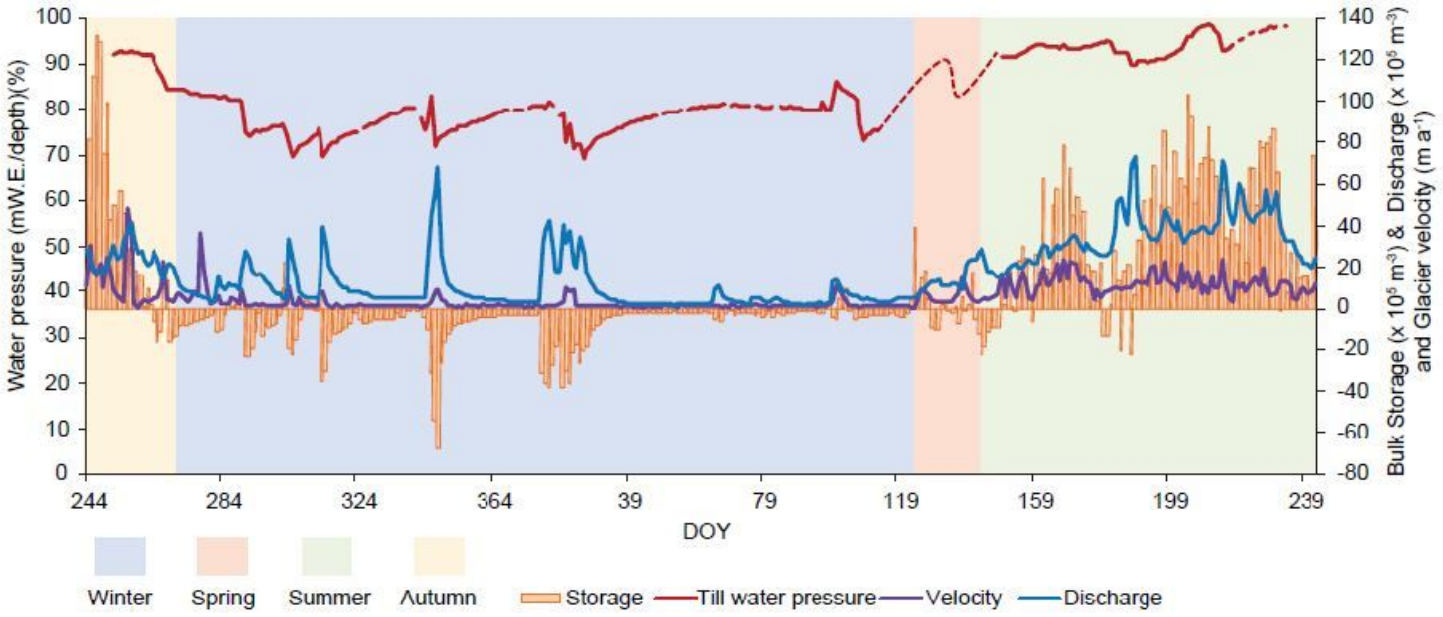

Figure 7

Composite annual bulk storage (melt minus discharge), till water pressure, melt and discharge from 2009/2010 data, velocity data estimated based on data from other years.

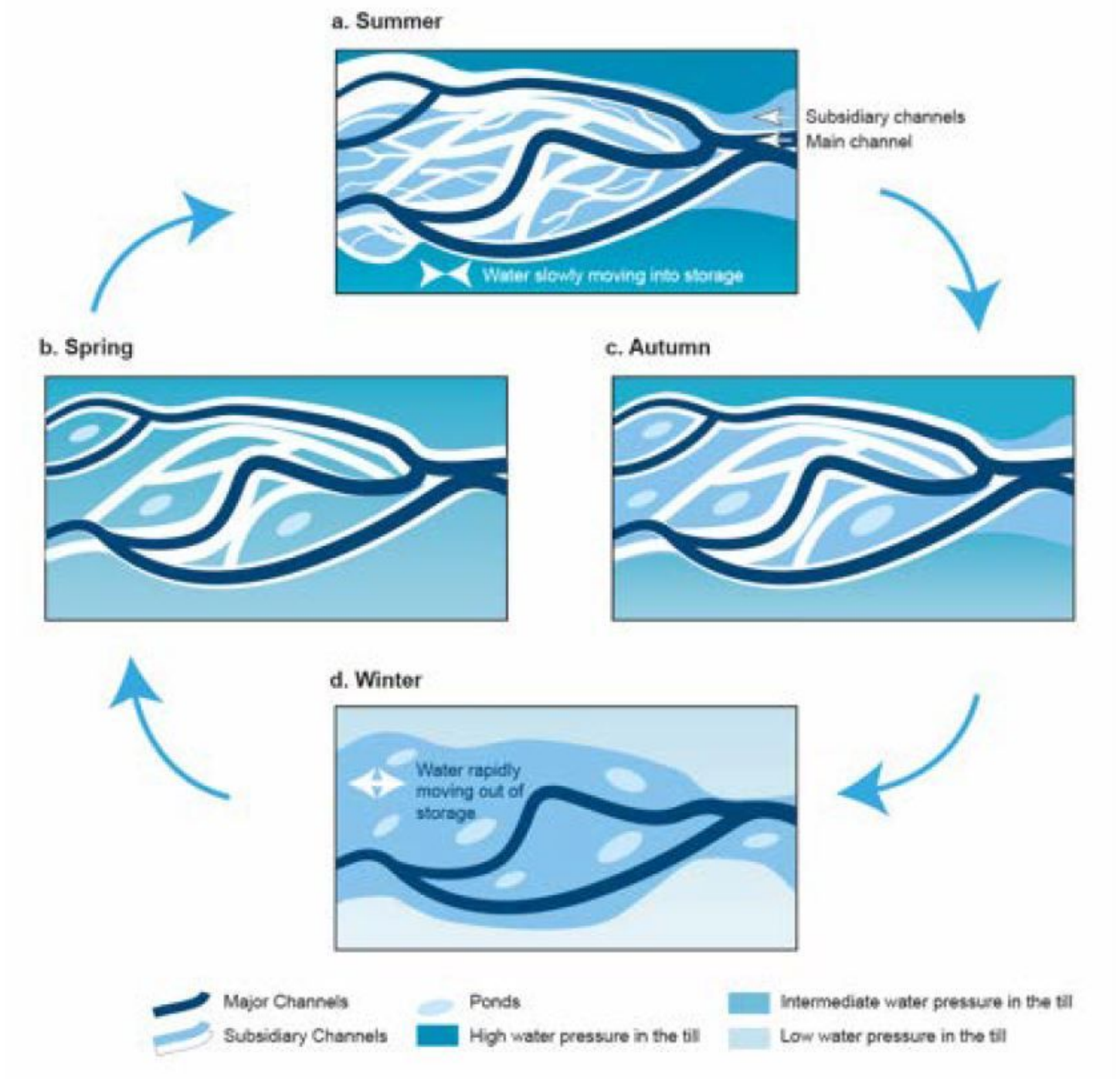

Figure 8

Model of the seasonal changes associated with anastomosing drainage: a) summer drainage, water is slowly transferred from one storage system to another, b & c) spring and autumn drainage, most water flows in the main channels, is some isolated small reservoirs; d) winter flow, during cold days, slow flow along main channels, during melt events, fast flow of water accessed from storage along a dominant channel.